

When Freeze-out Precedes Freeze-in: Sub-TeV Fermion Triplet Dark Matter with Radiative Neutrino Mass

Anirban Biswas,^a Debasish Borah,^{a,1} Dibyendu Nanda^a

^aDepartment of Physics, Indian Institute of Technology Guwahati, Assam 781039, India

E-mail: anirban.biswas.sinp@gmail.com, dborah@iitg.ac.in,
dibyendu.nanda@iitg.ac.in

Abstract. We propose a minimal predictive scenario for dark matter and radiative neutrino mass where the relic abundance of dark matter is generated from a hybrid setup comprising of both thermal freeze-out as well as non-thermal freeze-in mechanisms. Considering three copies of fermion triplets and one scalar doublet, odd under an unbroken \mathbb{Z}_2 symmetry, to be responsible for radiative origin of neutrino mass, we consider the lightest fermion triplet as a dark matter candidate which remains under-abundant in the sub-TeV regime from usual thermal freeze-out. Late decay of the \mathbb{Z}_2 -odd scalar doublet into dark matter serves as the non-thermal (freeze-in) contribution which not only fills the thermal dark matter deficit, but also constrains the mother particle's parameter space so that the correct relic abundance of dark matter is generated. Apart from showing interesting differences from the purely freeze-out and purely freeze-in dark matter scenarios, the model remains testable through disappearing charge track signatures at colliders, observable direct and indirect detection rates for dark matter and prediction of almost vanishing lightest neutrino mass.

¹Corresponding author

Contents

1	Introduction	1
2	Fermion Triplet Dark Matter (FTDM)	3
3	Scotogenic Extension of FTDM	5
4	Neutrino mass generation at one loop	8
5	Relic Abundance of dark matter candidate Σ_{1R}^0 in Scotogenic FTDM	9
6	LHC constraints on ψ_1^\pm	17
7	Direct Detection	19
8	Indirect Detection	21
9	Summary and Conclusion	22
A	Full calculation of the Lagrangian of fermionic triplet Σ	23

1 Introduction

There have been a convincing number of evidences from astrophysics and cosmology related experiments in the last several decades which suggest the presence of some non-baryonic and non-luminous form of matter, called dark matter (DM) in large amount distributed across the Universe. From the galaxy cluster observations by Fritz Zwicky [1] back in 1933, observations of galaxy rotation curves in 1970's [2], the more recent observation of the bullet cluster [3] and the latest cosmology data provided by the Planck satellite [4], it is now certain that around 27% of the present Universe is composed of such dark matter which is approximately five times more than the ordinary baryonic matter. The present abundance of DM is often quoted in terms of the density parameter Ω as [4]

$$\Omega_{\text{DM}}h^2 = \frac{\rho_{\text{DM}}}{\rho_c}h^2 = 0.1186 \pm 0.0020 \quad (1.1)$$

where $h = \frac{H_0}{100 \text{ km s}^{-1} \text{ Mpc}^{-1}}$ is a parameter of order unity while $H_0 = (67.8 \pm 0.9) \text{ km s}^{-1} \text{ Mpc}^{-1}$ [4], is the present value of the Hubble parameter and $\rho_c = \frac{3H_0^2}{8\pi G}$ is the critical density of the Universe with G being the universal constant of gravity. In spite of all these evidences, the particle nature of DM is not yet known leaving a wide range of possibilities. It is however, certain that none of the standard model (SM) particles can satisfy the requirements [5] of a typical DM candidate. This has led to several beyond standard model (BSM) proposals in the last few decades, the most popular of which being the so called weakly interacting massive particle (WIMP) paradigm. In this framework, a dark matter candidate typically with electroweak scale mass and interaction rate similar to electroweak interactions can give

rise to the correct dark matter relic abundance, a remarkable coincidence often referred to as the *WIMP Miracle*.

One interesting aspect of WIMP dark matter paradigm is their masses and interactions falling around the ballpark of the electroweak scale, which lead to their thermal production in the early Universe. The relic of such a particle arise when its interactions fall below the rate of expansion of the Universe, known as the freeze-out mechanism. These interactions between DM and SM particles leading to its thermal production in the early Universe can also lead to observable DM nucleon scattering cross sections. However, no such observations have so far been made which could have been a direct detection of particle DM. The most recent direct detection experiments like LUX, PandaX-II and XENON1T have also reported their null results [6–10]. The absence of such direct detection signals have progressively lowered the exclusion curve in DM-nucleon cross section versus DM mass plane. With such high precision measurements, the WIMP-nucleon cross section will soon overlap with the neutrino-nucleon cross section, known as the neutrino floor, making it difficult to distinguish a probable DM signal from the neutrino ones. Although such null results at direct detection frontier could indicate a very constrained region of WIMP parameter space, they have also motivated the particle physics community to seek for a paradigm shift. One such scenario that has drawn attention in the last few years is the non-thermal dark matter scenarios [11, 12]. In this case, the DM particles have so feeble interactions with the remaining thermal bath that it never attains thermal equilibrium at any epoch in the early Universe. However, it can be produced from decay of some heavy particles or scattering processes, popularly known as the freeze-in mechanism [12–15], leading to a new paradigm called freeze-in (or feebly interacting) massive particle (FIMP). For a recent review of this DM paradigm, please see [16].

Instead of completely giving up on the WIMP framework due to the null results at direct search experiments, here we consider a hybrid scenario where both thermal (freeze-out) and non-thermal (freeze-in) contributions to DM relic abundance can be important. To be more specific, DM can have sizeable interactions to be thermally produced in the early Universe but also needs a non-thermal source to satisfy the correct relic abundance in the present epoch. This idea was explored in several earlier works including [17–20] and references therein. Recently, such a work was performed for the inert Higgs doublet dark matter model [21] where the SM is extended by an additional scalar doublet odd under an in-built \mathbb{Z}_2 symmetry so that the lightest \mathbb{Z}_2 -odd component is a stable dark matter candidate. In that work the thermally under-abundant DM parameter space was revisited and it was shown that a non-thermal contribution from an additional \mathbb{Z}_2 -odd singlet neutral fermion can fill this deficit while the other two cousins of this singlet neutral fermion along with the inert scalar doublet can play a role in generating one loop radiative neutrino masses in scotogenic fashion [22]. It is worth mentioning at this point that the observation of non-zero neutrino masses and large leptonic mixing [23] has also been another motivation for BSM physics for last few decades. While the addition of singlet right handed neutrinos to the SM content can give rise to the usual seesaw mechanism [24–26] for neutrino mass at tree level, the scotogenic framework can explain the origin of neutrino mass and dark matter in a unified manner. In the earlier work [21] where both thermal and non-thermal contributions to scalar dark matter abundance were studied, the initial abundance of the heavy singlet fermion was not explained, but was fixed suitably in order to generate the required non-thermal contribution.

In the present work, we consider a more general study of this hybrid scenario within the framework of another minimal model for dark matter and neutrino masses but with more observable consequences. Here the singlet neutral fermions of the minimal scotogenic model

[22] are replaced by fermion triplets having zero hypercharge, but odd under the \mathbb{Z}_2 symmetry. As known from the discussions of fermion triplet dark matter (FTDM) model proposed by Ma and Suematsu [27], the fermion triplet dark matter is usually under-abundant below 2.2 TeV mass due to its large annihilation cross section. Inclusion of non-perturbative effects on dark matter annihilations [28, 29] which are more dominant for heavier dark matter masses, pushes this bound on fermion triplet DM mass to around 2.7 TeV [30]. In this work, we particularly focus on the fermion triplet dark matter mass around 1 TeV and check if a non-thermal contribution can fill the deficit coming from thermal freeze-out. In a scotogenic model with fermion triplet, the only non-thermal contribution for such 1 TeV DM can come from the \mathbb{Z}_2 odd scalar doublet. Unlike the earlier work [21] where the mother particle was a fermion singlet with tiny Yukawa coupling with the dark matter candidate, here the mother particle has gauge interactions and hence can have thermal abundance due to the usual freeze-out scenario. We solve the coupled Boltzmann equations corresponding to the comoving number densities of the inert scalar doublet as well as fermion triplets to determine the final relic abundance of fermion triplet DM. The inert scalar doublet, being heavier, freezes out first followed by the freeze-out of the fermion triplet. Then a non-thermal contribution from the inert scalar doublet fills the deficit in fermion triplet relic abundance from thermal freeze-out. The requirement for correct fermion triplet DM abundance not only constrains its coupling with the inert scalar doublet, but also the freeze-out abundance and hence the parameter space of the latter. The other two cousins of the fermion triplet dark matter can have sizeable coupling with inert scalar doublet and SM leptons to generate tiny neutrino masses at one loop. Since the lightest fermion triplet almost decouples from neutrino mass generation due to tiny Yukawa couplings (required for non-thermal production or freeze-in), the lightest neutrino remains massless in our scenario. We also check the testability of the model and find that such TeV scale fermion triplet DM can have observable consequences and direct, indirect dark matter detection experiments as well as collider experiments like the large hadron collider (LHC).

This paper is organised as follows. In section 2 we briefly discuss the fermion triplet dark matter followed by its scotogenic extension and details of the model we adopt for our present work in section 3. In section 4, we briefly discuss the generation of neutrino mass at one loop and then move on to discussing the details of dark matter relic calculation in section 5. We then discuss different constraints or observational aspects of our dark matter scenario at LHC, direct detection and indirect detection experiments in section 6, 7, 8 respectively. We finally conclude in section 9.

2 Fermion Triplet Dark Matter (FTDM)

In this section, we discuss a stable fermion triplet of zero hypercharge as a dark matter candidate, stabilised by an in-built \mathbb{Z}_2 symmetry. It is straightforward to realise the need of additional \mathbb{Z}_2 symmetry as otherwise the triplet can decay into the SM Higgs and lepton due to renormalizable couplings among them. A $SU(2)_L$ multiplet of higher dimensions can however be naturally stable without any need of additional symmetries, along the minimal dark matter spirit [31]. Fermion triplet dark matter was also studied by several other groups, the most recent of which can be found in [30] within the framework of another class of models. To be more technical, in a minimal setup of FTDM, the fermionic sector of the SM is extended by a $SU(2)_L$ triplet $\Sigma_R = (\Sigma_R^1 \ \Sigma_R^2 \ \Sigma_R^3)^T$ with zero hypercharge. The triplet Σ_R which is in the adjoint representation of $SU(2)_L$, can also be expressed in the fundamental representation

as

$$\Sigma_R = \frac{\sigma^i \Sigma_R^i}{\sqrt{2}} = \begin{pmatrix} \Sigma_R^0/\sqrt{2} & \Sigma_R^+ \\ \Sigma_R^- & -\Sigma_R^0/\sqrt{2} \end{pmatrix}, \quad (2.1)$$

where σ_i 's ($i = 1$ to 3) are the Pauli spin matrices, the generators of the fundamental representation of $SU(2)_L$ while $\Sigma_R^\pm = (\Sigma_R^1 \mp i \Sigma_R^2)/\sqrt{2}$, $\Sigma_R^0 = \Sigma_R^3$. Let us define $\Sigma = \Sigma_R + \Sigma_R^c$, where $\Sigma_R^c = C \overline{\Sigma_R}^T$ is the CP conjugate of Σ_R and C being the charge conjugation operator. Note that, by construction Σ is a Majorana fermion ($\Sigma^c = \Sigma$) however, not all the components of Σ are Majorana fermions. We have shown in the Appendix A that only neutral component of Σ is a Majorana fermion while the charged one is as usual a Dirac fermion. The Lagrangian of the triplet Σ is given by

$$\mathcal{L}_{triplet} = \frac{i}{2} \text{Tr}[\overline{\Sigma} \not{D} \Sigma] - \frac{1}{2} \text{Tr}[\overline{\Sigma} M_\Sigma \Sigma], \quad (2.2)$$

$$= \frac{i}{2} \text{Tr}[\overline{\Sigma}_R \not{D} \Sigma_R] + \frac{i}{2} \text{Tr}[\overline{\Sigma}_R^c \not{D} \Sigma_R^c] - \left(\frac{1}{2} \text{Tr}[\overline{\Sigma}_R^c M_\Sigma \Sigma_R] + h.c. \right), \quad (2.3)$$

where, D_μ is the covariant derivative of Σ_R and its expression is given in Eq. (A.3) of Appendix A. Now, inserting Eq. (2.1) into Eq. (2.3), and using the relation $\Sigma_R^c = C \overline{\Sigma_R}^T$, we get

$$\begin{aligned} \mathcal{L}_{triplet} = & \overline{\psi}^- i \not{D} \psi^- + \frac{1}{2} \overline{\psi}^0 i \not{D} \psi^0 - M_\Sigma \overline{\psi}^- \psi^- - \frac{M_\Sigma}{2} \overline{\psi}^0 \psi^0 - g \left(\overline{\psi}^- \gamma^\mu \psi^0 W_\mu^- + h.c. \right) \\ & + g \cos \theta_w \overline{\psi}^- \gamma_\mu \psi^- Z^\mu + g \sin \theta_w \overline{\psi}^- \gamma_\mu \psi^- A^\mu, \end{aligned} \quad (2.4)$$

where, we have defined $\psi^- = \Sigma_R^- + \Sigma_R^{+c}$, a four component Dirac spinor while ψ^0 is a Majorana fermion in four component notation as $\psi^0 = \Sigma_R^0 + \Sigma_R^{0c}$ and θ_w is the usual weak mixing angle known as the Weinberg angle. In Appendix A, we have explicitly derived Eq. (2.4) from Eq. (2.3). Now, if one introduces a \mathbb{Z}_2 parity on Σ_R then the neutral component ψ^0 , which is a Majorana fermion, can be a viable thermal dark matter candidate (WIMP). As the Yukawa interaction terms among Σ_R , SM leptons and Higgs boson are forbidden by the \mathbb{Z}_2 symmetry hence the DM candidate ψ^0 interacts with the SM particle only through gauge interactions. Moreover, from the Lagrangian (Eqs. (2.3), (2.4)) it is evident that the bare masses for all members of the fermionic triplet Σ_R are identical to M_Σ . However, one can make the charged components ψ^\pm heavier by considering one loop electroweak radiative corrections [27, 31], which result in a mass splitting ~ 166 MeV between M_{ψ^\pm} and M_{ψ^0} for $M_\Sigma \gtrsim 1$ TeV. In this framework, the relic density of the lightest \mathbb{Z}_2 -odd particle ψ^0 is determined by its pair annihilation into W^+W^- final state via t-channel exchange of ψ^\pm . Besides, the co-annihilations among ψ^0 and ψ^\pm into SM particles also play a crucial role in relic density calculation as the mass splitting between the members of the fermionic triplet is extremely small ($\sim \mathcal{O}(100$ MeV)). The co-annihilations include several process like $\psi^0 \psi^\pm \rightarrow W^\pm Z$ (via t-channel exchange of ψ^\mp), $\psi^+ \psi^- \rightarrow f \bar{f}$, W^+W^- (via s-channel exchange of Z), $\psi^\pm \psi^\pm (\psi^\mp) \rightarrow W^\pm W^\pm (W^\mp)$ (via t-channel exchange of ψ^0) etc. After including all these annihilation and co-annihilation channels, the relic density of ψ^0 satisfies the Planck limit [4] for $M_{\psi^0} \sim 2.2$ TeV [27] (see green dashed line in Fig. 4 in Section 5). Therefore, the dark matter mass allowed by the observational data from Planck satellite may not be produced efficiently in LHC at the present centre of mass energy and luminosity. This has also led to some recent discussions on fermion triplet dark matter with a singlet admixture, in order to lower the bound on fermion triplet from relic abundance point of view and to enhance

its production at colliders, see for example, [32]. It should be noted that such admixture of singlet fermion with the neutral component of fermion triplet as dark matter candidate was proposed long back by the authors of [33], motivated from its search prospects at LEP collider. We consider another minimal modifications of the present model which is also motivated from neutrino mass point of view, so that one can still have a much lighter triplet fermionic dark matter which at the same time satisfies all the existing direct and indirect bounds and can have tantalising detection prospects at the LHC. We will present a detailed discussion on this topic in Section 6.

3 Scotogenic Extension of FTDM

In order to have nonzero neutrino masses and a light triplet fermionic dark matter, we have extended the minimal model, described in the previous section, by two more triplets and one inert doublet. Therefore, besides the usual SM fields, the present model contains three fermionic $SU(2)_L$ triplets and one extra $SU(2)_L$ doublet $\Phi = \left(\phi^+ \quad \frac{\phi^0 + i A^0}{\sqrt{2}} \right)^T$. All these extra BSM fields are odd under the discrete symmetry \mathbb{Z}_2 . As a result, the Yukawa interaction terms involving fermionic triplet, SM Higgs doublet and lepton doublet are forbidden. Hence, one cannot generate tiny neutrino masses following usual Type-III seesaw mechanism [34–36], where the above mentioned Yukawa terms play a pivotal role. Instead, in the present model, we can write the Yukawa terms using the inert Higgs doublet Φ . However, the extra doublet Φ , being an inert one (does not interact with SM fermions), does not have any vacuum expectation value (VEV) (in order to maintain \mathbb{Z}_2 symmetry unbroken). Hence, there are no neutrino masses at tree level (Type-III seesaw is not possible) and instead, the light neutrino masses can be generated radiatively at one loop level following the scotogenic model [22]. This scotogenic version of Type-III seesaw model is also known as radiative Type-III seesaw model, studied in different contexts by several authors [27, 37, 38].

Further, the Majorana type bare mass terms $\text{Tr} \left[\overline{\Sigma_{\alpha R}^c} M_{\Sigma}^{\alpha\beta} \Sigma_{\beta R} \right]$ are although invariant under \mathbb{Z}_2 symmetry, the origin of such terms is not obvious in the present scenario. Therefore, to understand a possible origin of bare mass term of fermionic triplet we introduce a scalar field S' , which is a singlet under SM gauge group. Moreover, we also impose an additional \mathbb{Z}_3 charges to $\Sigma_{\beta R}$ ($\beta = 1$ to 3) and S' such that the bare mass term of $\Sigma_{\beta R}$ is forbidden by \mathbb{Z}_3 symmetry while at the same time $\text{Tr} \left[\overline{\Sigma_{\alpha R}^c} y_s^{\alpha\beta} \Sigma_{\beta R} \right] S'^{\dagger}$ term is allowed. Thus, when S' gets a VEV, $\langle S' \rangle = \frac{v_s}{\sqrt{2}}$, this term will generate the bare mass term $M_{\Sigma}^{\alpha\beta} \sim y_s^{\alpha\beta} v_s$. Apart from that the singlet scalar S' also helps the present model to evade the indirect detection bounds on W^+W^- annihilation channel [39]. This limit is obtained from the non-observation of excess gamma-rays, over the known backgrounds, due to dark matter annihilation from dwarf spheroidal galaxies. Another interesting aspect of including this singlet scalar is to enhance the dark matter direct detection rate by introducing a tree level scattering while the minimal model had only radiative direct detection scattering at one loop level. We will have a detailed discussion on this topic in Section 8. Furthermore, we have to impose appropriate \mathbb{Z}_3 charges to the SM leptons as well so that the Yukawa interaction terms involving both inert doublet Φ and SM Higgs doublet H remain invariant under \mathbb{Z}_3 symmetry. The \mathbb{Z}_3 charges of $\Sigma_{\beta R}$ and SM leptons can be ω^2 while that of S' can be ω , where ω^2, ω are the cube roots of unity.

The Lagrangian involving $\Sigma_{\beta R}$, Φ and S' fields, which is invariant under $SU(2)_L \times U(1)_Y \times \mathbb{Z}_2 \times \mathbb{Z}_3$ symmetry, is given by

$$\begin{aligned} \mathcal{L}_{\text{BSM}} \supset & \frac{i}{2} \left(\sum_{\beta=1}^3 \text{Tr}[\overline{\Sigma_{\beta R}} \not{D} \Sigma_{\beta R}] + \text{Tr}[\overline{\Sigma_{\beta R}^c} \not{D} \Sigma_{\beta R}^c] \right) - \left(\sum_{\alpha, \beta=1}^3 \frac{1}{2} \text{Tr}[\overline{\Sigma_{\alpha R}^c} \sqrt{2} y_s^{\alpha\beta} \Sigma_{\beta R}] S'^{\dagger} + h.c. \right) \\ & - \left(\sum_{\alpha, \beta=1}^3 y_{\Sigma}^{\alpha\beta} \overline{l_{\alpha L}} \Sigma_{\beta R} \tilde{\Phi} + h.c. \right) + \mathcal{L}_{\text{scalar}}(H, \Phi, S'), \end{aligned} \quad (3.1)$$

where $\tilde{\Phi} = i\sigma_2 \Phi^*$ and the Lagrangian for the scalar fields are given by

$$\begin{aligned} \mathcal{L}_{\text{scalar}}(H, \Phi, S') = & (D_{\mu} H)^{\dagger} (D^{\mu} H) + (D_{\mu} \Phi)^{\dagger} (D^{\mu} \Phi) + \partial_{\mu} S'^{\dagger} \partial^{\mu} S' + \mu_H^2 H^{\dagger} H - \lambda_H (H^{\dagger} H)^2 \\ & - \mu_2^2 \Phi^{\dagger} \Phi - \lambda_2 (\Phi^{\dagger} \Phi)^2 + \mu_s^2 S'^{\dagger} S' - \mu_3 (S'^3 + S'^{\dagger 3}) - \lambda_s (S'^{\dagger} S')^2 \\ & - \lambda_3 (H^{\dagger} H) (\Phi^{\dagger} \Phi) - \lambda_4 (H^{\dagger} \Phi) (\Phi^{\dagger} H) - \frac{\lambda_5}{2} ((H^{\dagger} \Phi)^2 + h.c.) \\ & - \lambda_6 (H^{\dagger} H) (S'^{\dagger} S') - \lambda_7 (\Phi^{\dagger} \Phi) (S'^{\dagger} S'). \end{aligned} \quad (3.2)$$

where $S' = \frac{h_2 + i\zeta}{\sqrt{2}}$, h_2 and ζ are the real and imaginary parts of S' respectively while $H = \begin{pmatrix} 0 \\ \frac{h_1 + iv}{\sqrt{2}} \end{pmatrix}^T$ is the SM Higgs doublet in the unitary gauge. Following the procedure given in the Appendix A, we can write the triplet Lagrangian in terms of $\psi_{\beta}^{-} = \Sigma_{\beta R}^{-} + \Sigma_{\beta R}^{+c}$ and $\psi_{\beta}^0 = \Sigma_{\beta R}^0 + \Sigma_{\beta R}^{0c}$ as

$$\begin{aligned} \mathcal{L}_{\text{BSM}} \supset & \sum_{\beta=1}^3 \overline{\psi_{\beta}^{-}} i \not{D} \psi_{\beta}^{-} + \frac{1}{2} \overline{\psi_{\beta}^0} i \not{D} \psi_{\beta}^0 - \left(\sum_{\alpha, \beta=1}^3 y_s^{\alpha\beta} \overline{\psi_{\alpha}^{-}} \psi_{\beta}^{-} + \frac{y_s^{\alpha\beta}}{2} \overline{\psi_{\alpha}^0} \psi_{\beta}^0 \right) h_2 \\ & - i \left(\sum_{\alpha, \beta=1}^3 y_s^{\alpha\beta} \overline{\psi_{\alpha}^{-}} \gamma_5 \psi_{\beta}^{-} + \frac{y_s^{\alpha\beta}}{2} \overline{\psi_{\alpha}^0} \gamma_5 \psi_{\beta}^0 \right) \zeta - g \left(\overline{\psi_{\beta}^{-}} \gamma^{\mu} \psi_{\beta}^0 W_{\mu}^{-} + h.c. \right) \\ & + g \cos \theta_w \overline{\psi_{\beta}^{-}} \gamma_{\mu} \psi_{\beta}^{-} Z^{\mu} + g \sin \theta_w \overline{\psi_{\beta}^{-}} \gamma_{\mu} \psi_{\beta}^{-} A^{\mu} \\ & - \left[\sum_{\alpha, \beta=1}^3 y_{\Sigma}^{\alpha\beta} \left(\frac{1}{\sqrt{2}} \overline{\nu_{\alpha L}} P_R \psi_{\beta}^0 + \overline{e_{\alpha L}} P_R \psi_{\beta}^{-} \right) \left(\frac{\phi^0 - i A^0}{\sqrt{2}} \right) - y_{\Sigma}^{\alpha\beta} \overline{P_L \psi_{\beta}^{-}} \nu_{\alpha L}^c \phi^{-} \right. \\ & \left. + \frac{y_{\Sigma}^{\alpha\beta}}{\sqrt{2}} \overline{e_{\alpha L}} P_R \psi_{\beta}^0 \phi^{-} + h.c. \right] + \mathcal{L}_{\text{scalar}}(H, \Phi, S'). \end{aligned} \quad (3.3)$$

As mentioned earlier, when the real part of S' gets VEV v_s , the mass terms for both ψ_{α}^{-} and ψ_{α}^0 are generated from the third and fourth terms of the above Lagrangian as $M_{\psi}^{\alpha\beta} = y_s^{\alpha\beta} v_s$. For simplicity, we have assumed that $M_{\psi}^{\alpha\beta}$ is a diagonal matrix with real and nonzero elements. Therefore, both ψ_{α}^0 and ψ_{α}^{-} are representing the physical states and the lightest neutral fermion ψ_1^0 can be our dark matter candidate with mass $M_{\psi_1^0} = y_s v_s$ ¹. Furthermore, the

¹For notational simplicity we choose $y_s^{11} = y_s$.

first term within the square bracket is responsible for tiny neutrino mass generation at one loop level. We will have a detailed discussion on this topic in the next section (Section 4). After $SU(2)_L \times U(1)_Y \times \mathbb{Z}_3$ symmetry breaking, the mass terms for the components of inert Higgs doublet are

$$M_{\phi^\pm}^2 = \mu_2^2 + \frac{1}{2} (\lambda_3 v^2 + \lambda_7 v_s^2) , \quad (3.4)$$

$$M_{A^0}^2 = \mu_2^2 + \frac{1}{2} [(\lambda_3 + \lambda_4 - \lambda_5) v^2 + \lambda_7 v_s^2] , \quad (3.5)$$

$$M_{\phi^0}^2 = \mu_2^2 + \frac{1}{2} [(\lambda_3 + \lambda_4 + \lambda_5) v^2 + \lambda_7 v_s^2] . \quad (3.6)$$

On the other hand, after symmetry breaking there will be a mixing between the real scalar fields of H and S' . The mixing matrix with respect to the basis (h_1, h_2) is given by

$$\mathcal{M}_{\text{scalar}}^2 = \begin{pmatrix} 2\lambda_H v^2 & \lambda_6 v v_s \\ \lambda_6 v v_s & 2\lambda_s v_s^2 + \frac{3\mu_3 v_s}{\sqrt{2}} \end{pmatrix} . \quad (3.7)$$

Clearly, h_1 and h_2 do not represent physical fields. However, after diagonalising the above mass matrix, one can have two physical scalar fields h and S , which are two orthogonal linear combinations of h_1, h_2 and the corresponding mixing angle is given by

$$\tan 2\xi = \frac{\lambda_6 v v_s}{\lambda_H v^2 - \lambda_s v_s^2 - \frac{3\mu_3 v_s}{2\sqrt{2}}} . \quad (3.8)$$

We consider h is the SM-Like Higgs boson which was discovered at the LHC [40, 41]. The mass of the pseudo scalar ζ is given by

$$M_\zeta^2 = -\frac{3\mu_3 v_s}{\sqrt{2}} , \quad (3.9)$$

where we need $\mu_3 < 0$ for $M_\zeta^2 > 0$. The trilinear terms of S' and S'^\dagger allowed by \mathbb{Z}_3 symmetry play a crucial role in generating the mass term for the imaginary part of S' after spontaneous symmetry breaking of \mathbb{Z}_3 . As a result, we can choose the mass of the pseudo scalar (ζ) different than S and also heavier compared to the mass of our dark matter candidate ψ_1^0 , so that it will not affect the relic density of ψ_1^0 . From Eqs. (3.9), one can easily find that

M_ζ will be heavier than our dark matter candidate ψ_1^0 when $\mu_3 < -\frac{\sqrt{2} M_{\psi_1^0}^2}{3 v_s}$. Now, using

$M_{\psi_1^0} = y_s v_s$, we can rewrite the above limit on μ_3 as $\mu_3 < -\frac{\sqrt{2} y_s^2}{3} v_s$. On the other hand, since μ_3 acts oppositely to the expression of M_s , therefore one can also find a lower bound on self coupling λ_s from the requirement of $M_s > 0$. Therefore, under the approximation of small mixing angle ξ , the quartic coupling λ_s must be greater than $\frac{y_s^2}{2}$. In Sections 5 and 8, we have considered $y_s = 1.5$ for $M_{\psi_1^0} = 1$ TeV and hence we need $\mu_3 < -707.11$ GeV and $\lambda_s > 1.13$. One thing we want to note here that the considered hierarchy $M_\zeta > M_{\psi_1^0} > M_s$ is solely for the calculational simplification. There may be a situation when $M_{\psi_1^0} > M_\zeta, M_s$, where our dark matter candidate can annihilate to both ζ as well as S and in that case due to the extra annihilation modes, the thermal contribution to dark matter relic abundance

will be even less compared to the present scenario. The main difference between the minimal model discussed in the previous section and the present model is that here, our dark matter candidate ψ_1^0 , after its thermal freeze-out, gets some non-thermal contribution to the relic abundance mainly from the decay of ϕ^0 . This eventually compensates the under abundance of ψ_1^0 in low mass regime $M_{\psi_1} \lesssim 2$ TeV. We also consider the mass of ϕ^0 to be smaller than the heavier cousins of Σ_{1R} so that ϕ^0 decays preferentially to the dark matter candidate only. This is also important from the point of view of neutrino mass (as we discuss in the next section) because the couplings of $\Sigma_{2R,3R}$ with Φ and SM leptons have to be sizeable in order to generate the correct one loop neutrino mass at sub-eV. Therefore, if $\Sigma_{2R,3R}$ are lighter than Φ , then ϕ^0 will also decay into these triplets reducing the branching ratio into the dark matter candidate Σ_{1R} , falling short of providing the required non-thermal contribution. We will discuss in great detail about the thermal as well as non-thermal contributions to the relic density of our dark matter candidate in Section 5.

4 Neutrino mass generation at one loop

In the present model since we have imposed both \mathbb{Z}_2 as well as \mathbb{Z}_3 charges to all three fermion triplets $\Sigma_{\beta R}$, neutrino masses can not be generated via tree level Type-III seesaw mechanism. However, in this model we have an inert doublet Φ which is also odd under \mathbb{Z}_2 symmetry. Hence we can write a Yukawa interaction term involving fermion triplet $\Sigma_{\beta R}$ inert doublet Φ and SM lepton doublet $l_{\alpha L}$. Such term will be automatically \mathbb{Z}_2 invariant. However, \mathbb{Z}_3 invariance requires same \mathbb{Z}_3 charge to SM leptons as well since Φ does not have any \mathbb{Z}_3 charge. Because, any nonzero \mathbb{Z}_3 charge of Φ , other than unity, will forbid the mass splitting between A^0 and ϕ^0 , which is $\lambda_5 v^2$ (see Eqs. (3.5 and 3.6)). Later in this section, we will see that the light neutrino masses are proportional to the mass splitting between A^0 and ϕ^0 , hence we cannot impose any non-trivial \mathbb{Z}_3 charge to Φ . Therefore, in this work as mentioned in the previous section, we choose \mathbb{Z}_3 charge of $\Sigma_{\beta R}$ and $l_{\alpha L}$ is ω^2 . The Yukawa interaction terms invariant under both continuous and discrete symmetries of the model are given as

$$\begin{aligned} \mathcal{L}_{\text{Yukawa}} \supset & - \sum_{\alpha, \beta=1}^3 y_{\Sigma}^{\alpha\beta} \overline{l_{\alpha L}} \Sigma_{\beta R} \tilde{\Phi} + h.c. , \\ & - \sum_{\alpha, \beta=1}^3 y_{\Sigma}^{\alpha\beta} \left(\frac{1}{\sqrt{2}} \overline{\nu_{\alpha L}} P_R \psi_{\beta}^0 + \overline{e_{\alpha L}} P_R \psi_{\beta}^{-} \right) \left(\frac{\phi^0 - i A^0}{\sqrt{2}} \right) - y_{\Sigma}^{\alpha\beta} \overline{P_L \psi_{\beta}^{-}} \nu_{\alpha L}^c \phi^{-} \\ & + \frac{y_{\Sigma}^{\alpha\beta}}{\sqrt{2}} \overline{e_{\alpha L}} P_R \psi_{\beta}^0 \phi^{-} + h.c. , \end{aligned} \quad (4.1)$$

where we have used the definition of ψ_{β}^{-} and ψ_{β}^0 give in Appendix A. As discussed in previous section, the first term in the above Lagrangian is responsible for neutrino mass generation in one loop level following the scotogenic model [22]. The Feynman diagram for neutrino mass generation at one loop level is shown in Fig. 1. In Fig. 1, we have drawn the diagram with ϕ^0 as an intermediate loop particle. However, the same diagram with ϕ^0 replaced by pseudo scalar A^0 is also possible. These two diagrams will differ by a -ve sign which actually helps us to cancel the divergences of both diagrams. The expression of neutrino mass is then given by [22]

$$\mathcal{M}_{\nu}^{\alpha\beta} = \sum_{\rho} \frac{y_{\Sigma}^{\alpha\rho} y_{\Sigma}^{\beta\rho} M_{\psi_{\rho}^0}}{64\pi^2} \left(\frac{M_{\phi^0}^2}{M_{\phi^0}^2 - M_{\psi_{\rho}^0}^2} \ln \frac{M_{\phi^0}^2}{M_{\psi_{\rho}^0}^2} - \frac{M_{A^0}^2}{M_{A^0}^2 - M_{\psi_{\rho}^0}^2} \ln \frac{M_{A^0}^2}{M_{\psi_{\rho}^0}^2} \right). \quad (4.2)$$

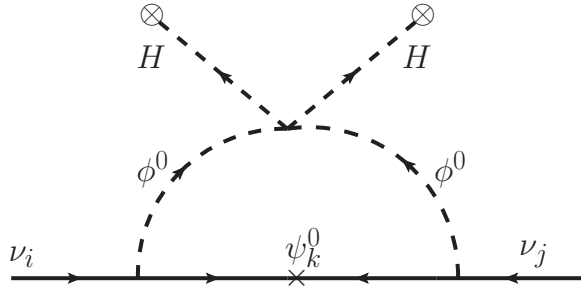


Figure 1. Feynman diagram of neutrino mass generation at one loop.

Now, if we consider the mass splitting between M_A^0 and M_{ϕ^0} is small compared to $(M_A^0 + M_{\phi^0})/2$, which is indeed true for our work (see Section 5), the expression for $\alpha\beta$ element of neutrino mass matrix simplifies to

$$\mathcal{M}_\nu^{\alpha\beta} = \frac{\lambda_5 v^2}{64\pi^2} \sum_\rho \frac{y_\Sigma^{\alpha\rho} y_\Sigma^{\beta\rho} M_{\psi_\rho^0}}{M_0^2 - M_{\psi_\rho^0}^2} \left(1 - \frac{M_{\psi_\rho^0}^2}{M_0^2 - M_{\psi_\rho^0}^2} \ln \frac{M_0^2}{M_{\psi_\rho^0}^2} \right), \quad (4.3)$$

where $M_0^2 = (M_A^0 + M_{\phi^0})/2$ and $M_{A^0}^2 - M_{\phi^0}^2 = \lambda_5 v^2$ using Eqs. (3.5 and 3.6). It should be noted that the requirement for non-thermal contribution to dark matter candidate in our model constrains the Yukawa couplings of the lightest fermion triplet with the SM leptons to be very small $y_\Sigma^{11} \approx y_\Sigma^{21} \approx y_\Sigma^{31} \leq 10^{-9}$, as we discuss in details below. As can be seen from the one loop neutrino mass formula given above, such tiny couplings will practically have a negligible contribution to light neutrino masses. This makes the lightest fermion triplet to effectively decouple from the neutrino mass generation mechanism giving rise to one almost massless and two massive light neutrinos which can be tested at experiments which are sensitive to the absolute mass scale of neutrinos.

5 Relic Abundance of dark matter candidate Σ_{1R}^0 in Scotogenic FTDM

To compute the relic abundance of a dark matter candidate, one has to find the value of comoving number density of dark matter species at the present epoch, which can be found by solving the corresponding Boltzmann equation for the dark matter candidate we are considering i.e. ψ_1^0 . Moreover, while solving the Boltzmann equation for ψ_1^0 , we need to have the information about the comoving number densities of other particles which are not in thermal equilibrium but have significant impact on the production processes of ψ_1^0 . In other words, we need to solve a system of coupled Boltzmann equations for all the out of equilibrium particles.

The coupled Boltzmann equations for our present scenario are given by

$$\begin{aligned} \frac{dY_{\psi_1^0}}{dx} = & - \left(\frac{45 G}{\pi} \right)^{-1/2} \frac{M_{sc}}{x^2} \sqrt{g_\star} \langle \sigma v \rangle_{\text{Triplet}} \left(Y_{\psi_1^0}^2 - (Y_{\psi_1^0}^{eq})^2 \right) \\ & + \left(\frac{4\pi^3 G}{45} \right)^{-1/2} \frac{x}{M_{sc}^2} \frac{\sqrt{g_\star}}{g_s} \left(\langle \Gamma_{\phi^0 \rightarrow \psi_1^0} \rangle Y_{\phi^0} + 2 \langle \Gamma_{\psi_1^\pm \rightarrow \psi_1^0} \rangle Y_{\psi_1^\pm} \right), \end{aligned} \quad (5.1)$$

$$\begin{aligned} \frac{dY_{\phi^0}}{dx} = & - \left(\frac{45 G}{\pi} \right)^{-1/2} \frac{M_{sc}}{x^2} \sqrt{g_\star} \langle \sigma v \rangle_{\text{IDM}} \left(Y_{\phi^0}^2 - (Y_{\phi^0}^{eq})^2 \right) \\ & - \left(\frac{4\pi^3 G}{45} \right)^{-1/2} \frac{x}{M_{sc}^2} \frac{\sqrt{g_\star}}{g_s} \langle \Gamma_{\phi^0}^{\text{Total}} \rangle Y_{\phi^0}, \end{aligned} \quad (5.2)$$

$$\frac{dY_{\psi_1^-}}{dx} = \left(\frac{4\pi^3 G}{45} \right)^{-1/2} \frac{x}{M_{sc}^2} \frac{\sqrt{g_\star}}{g_s} \left(\langle \Gamma_{\phi^0 \rightarrow \psi_1^-} \rangle Y_{\phi^0} - \langle \Gamma_{\psi_1^- \rightarrow \psi_1^0} \rangle Y_{\psi_1^-} \right), \quad (5.3)$$

where, M_{sc} is some arbitrary mass scale and here we have considered $M_{sc} = M_{\psi_1^0}$. The first Boltzmann equation describes the evolution of comoving number density of ψ_1^0 where the first term in the R.H.S. represents the thermal WIMP contribution to $Y_{\psi_1^0}$ coming from the annihilations and co-annihilations among the ψ_1^0 and ψ_1^\pm . As mentioned earlier, since the mass splitting between ψ_1^\pm and ψ_1^0 is $\sim \mathcal{O}(100 \text{ MeV})$, the effect of co-annihilations [42, 43] is significant to $Y_{\psi_1^0}$. In Eq. (5.1), $\langle \sigma v \rangle_{\text{Triplet}}$ is the thermally averaged cross section for the annihilation and co-annihilation channels which are contributing significantly to the freeze-out process of ψ_1^0 . The Feynman diagrams of these processes are shown in Fig. 2. It is worth mentioning that we are not taking any non-perturbative effects on DM annihilations into account here which is justified by the fact that such effects are small for DM masses in the sub TeV regime [28, 29]. This is in fact, another motivation for confining our discussion to the sub-TeV mass regime of dark matter. Here, we have considered the mass difference between ψ_1^0 and other heavier triplet fermions ($\psi_\beta^0, \psi_\beta^\pm, \beta = 2, 3$) to be large so that the co-annihilations of these heavier triplet fermions do not affect the freeze-out process of ψ_1^0 .

The second term in the R.H.S. of Eq. (5.1), which appears with an opposite sign to the first one, is the non-thermal contributions to $Y_{\psi_1^0}$ coming from the decays of ϕ^0 and ψ_1^\pm and the corresponding thermal averaged decay widths are indicated by $\langle \Gamma_{\phi^0 \rightarrow \psi_1^0} \rangle$ and $\langle \Gamma_{\psi_1^\pm \rightarrow \psi_1^0} \rangle$ respectively. The general expression of thermal averaged decay width for a decay process $A \rightarrow BC$ is $\langle \Gamma_{A \rightarrow BC} \rangle = \Gamma_{A \rightarrow BC} \frac{K_1(\frac{M_A}{T})}{K_2(\frac{M_A}{T})}$, where M_A is the mass of the mother particle A and K_n is the n th order Modified Bessel function of second kind. These non-thermal contributions proportional to the thermal averaged decay widths $\langle \Gamma_{\phi^0 \rightarrow \psi_1^0} \rangle$ and $\langle \Gamma_{\psi_1^\pm \rightarrow \psi_1^0} \rangle$ respectively, are effective only after the freeze-out of ψ_1^0 before which ψ_1^0 has equilibrium number density governed by the Maxwell-Boltzmann distribution function. The decay of $\phi^0 \rightarrow \psi_1^0 \nu$ is due to the Yukawa interaction (first term within the square bracket of Eq. (3.3)), which is also responsible for the neutrino mass generation radiatively, while the decay of $\psi_1^\pm \rightarrow \psi_1^0 \pi^\pm$ is possible due to an $\mathcal{O}(100 \text{ MeV})$ mass splitting between ψ_1^\pm and ψ_1^0 . Although, ψ_1^\pm has some three-body decay modes like $\psi_1^{+(-)} \rightarrow \psi_1^0 + \bar{l}(l) + \nu(\bar{\nu})$ and $\psi_1^{+(-)} \rightarrow \psi_1^0 + u(\bar{u}) + \bar{d}(d)$, $\psi_1^\pm \rightarrow \psi_1^0 \pi^\pm$ is the dominant decay mode of charged fermion ψ_1^\pm with nearly 97% branching

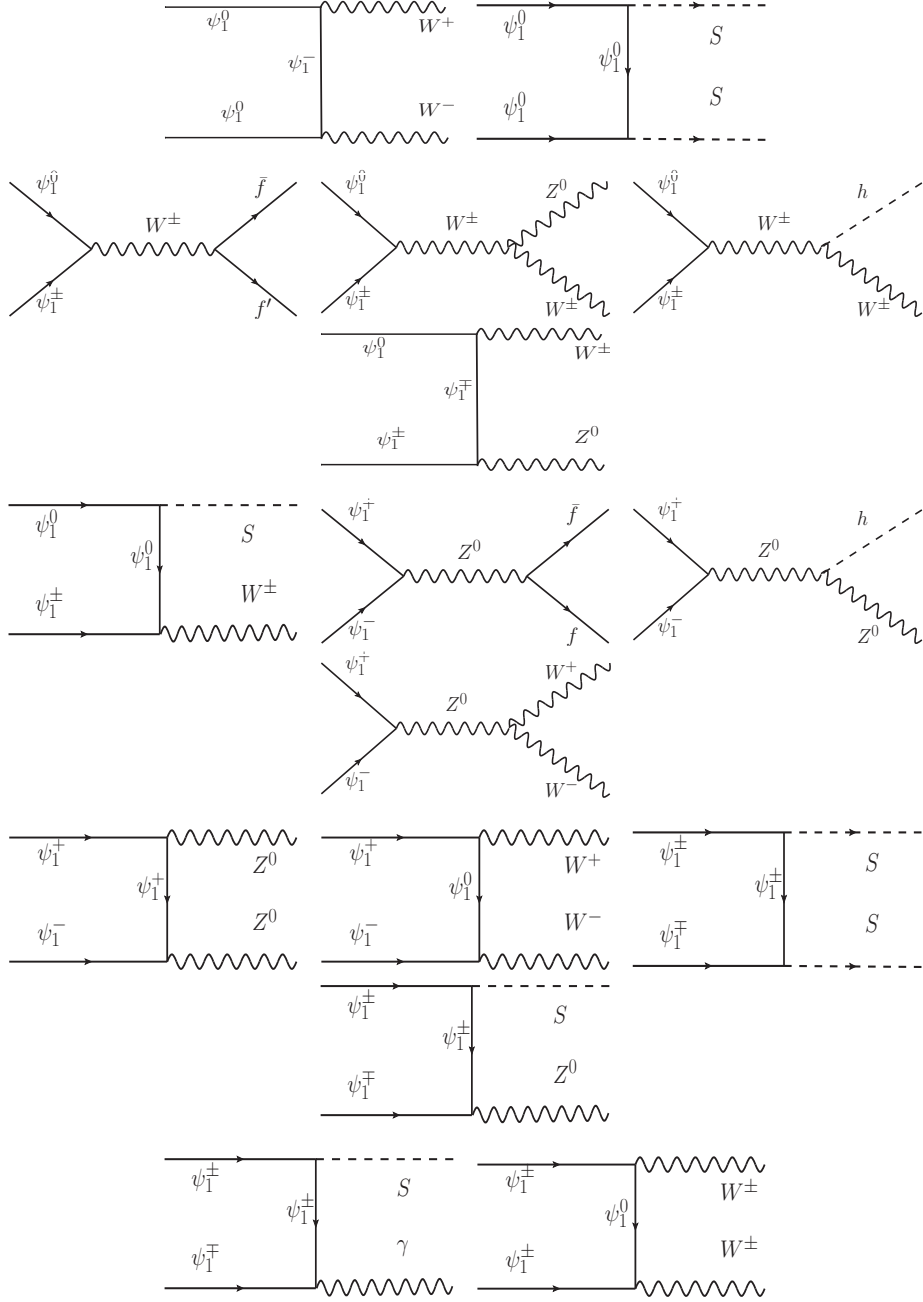


Figure 2. Feynman diagrams for all possible annihilation and co-annihilation channels. Two diagrams in first row are annihilation of ψ_1^0 while rest are co-annihilations.

ratio [31]. The expression of decay width for $\psi_1^\pm \rightarrow \psi_1^0 \pi^\pm$ is given by

$$\Gamma_{\psi_1^\pm \rightarrow \psi_1^0} = \frac{g^4 f_\pi^2 V_{ud}^2}{128\pi M_W^4 M_{\psi_1^\pm}} \Delta M_{\text{triplet}}^2 \left((M_{\psi_1^0} + M_{\psi_1^\pm})^2 - M_\pi^2 \right) \times \sqrt{1 - \frac{(M_{\psi_1^0} - M_\pi)^2}{M_{\psi_1^\pm}^2}} \sqrt{1 - \frac{(M_{\psi_1^0} + M_\pi)^2}{M_{\psi_1^\pm}^2}}, \quad (5.4)$$

where $\Delta M_{\text{triplet}} = M_{\psi_1^\pm} - M_{\psi_1^0} \simeq 166$ MeV, g is the $SU(2)_L$ gauge coupling, the pion decay constant $f_\pi = 131$ MeV [31] and the first diagonal element of the CKM matrix $V_{ud} \simeq 0.974$ respectively. Since we have assumed that there is no asymmetry between the comoving number densities of ψ_1^+ and ψ_1^- and decay widths $\Gamma_{\psi_1^- \rightarrow \psi_1^0} = \Gamma_{\psi_1^+ \rightarrow \psi_1^0} = \Gamma_{\psi_1^\pm \rightarrow \psi_1^0}$, the non-thermal contribution arising from the decays of ψ_1^+ and ψ_1^- are equal. Therefore, without explicitly showing the contribution of ψ_1^+ in $Y_{\psi_1^0}$, we have multiplied the term for ψ_1^- in Eq. (5.1) by a factor of 2.

The second Boltzmann equation in Eq. (5.2), is the evolution equation for ϕ_0 . In the R.H.S. of this equation, the first term is the collision term due to the annihilation and co-annihilation processes among the components of inert doublet Φ . These processes were in both thermal as well as chemical equilibrium in the early Universe and the lightest neutral component ϕ^0 of Φ freezes-out when these interaction rates become less than the expansion rate of the Universe, which is governed by the Hubble parameter $\mathbf{H}(T)$. The effective annihilation cross section, which we have denoted by $\langle\sigma v\rangle_{\text{IDM}}$ for ϕ^0 and $\langle\sigma v\rangle_{\text{Triplet}}$ for ψ_1^0 respectively, can be expressed as a weighted sum of individual annihilation and co-annihilation cross sections [42]. We have calculated $\langle\sigma v\rangle_{\text{IDM}}$ using `micrOMEGAs` package [44]. In the present scenario, although ϕ^0 has a \mathbb{Z}_2 charge, it is not the lightest \mathbb{Z}_2 -odd particle in the model. Hence, it can decay to other lighter \mathbb{Z}_2 -odd particles such as ψ_1^\pm , ψ_1^0 ². These decay modes further decrease the number density of ϕ^0 after its thermal freeze-out and this effect has been included in the Boltzmann equation of ϕ^0 by the second term in the R.H.S. of Eq. (5.2), which is, as expected, proportional to the total decay width $\Gamma_{\phi^0}^{\text{Total}}$ of ϕ^0 . Finally, Eq. (5.3) is the Boltzmann Equation for ψ_1^- . As we know that after the freeze-out of ψ_1^0 , the abundance of ψ_1^\pm is zero. However, ψ_1^\pm can again be produced from the late decay of ϕ^0 and those ψ_1^\pm eventually decay to ψ_1^0 and contribute to the non-thermal abundance of ψ_1^0 . In the R.H.S. of Eq. (5.3), the first term is the production term of ψ_1^- from the decay of ϕ^0 while the second one with an opposite sign is the depletion term of ψ_1^- . Like ψ_1^- , one can also write a same Boltzmann equation for ψ_1^+ as well, however since both ψ_1^+ and ψ_1^- have identical interactions with other particles and also we have assumed that there is no asymmetry in the initial number densities of ψ_1^+ and ψ_1^- , hence we do not need to solve an extra Boltzmann equation similar to Eq. (5.3) for ψ_1^+ . Ultimately, we have solved three coupled Boltzmann equations given in Eqs. (5.1-5.3) numerically to find the comoving number density $Y_{\psi_1^0}(T_0)$ of ψ_1^0 at the present epoch, which contains both thermal as well as non-thermal contributions. Finally, the relic density of our dark matter candidate ψ_1^0 can be computed from the value of $Y_{\psi_1^0}(T_0)$ using the following relation [43]

$$\Omega_{\psi_1^0} h^2 = 2.755 \times 10^8 \left(\frac{M_{\psi_1^0}}{\text{GeV}} \right) Y_{\psi_1^0}(T_0), \quad (5.5)$$

where $T_0 \simeq 2.73$ K, the present temperature of the Universe.

In the left panel of Fig. 3, we show the variation of comoving number densities of ϕ^0 , ψ_1^0 and ψ_1^\pm with $x = \frac{M_{\psi_1^0}}{T}$. Here, the variation of Y_{ϕ^0} is denoted by green solid line and as mentioned above due to the finite decay width $\Gamma_{\phi^0}^{\text{Total}}$, the comoving number density of ϕ^0 , instead of becoming a constant with temperature T , decreases sharply after its freeze-out. Due to this decrement of Y_{ϕ^0} there is an increment in $Y_{\psi_1^0}$ denoted by red solid line as more and more ψ_1^0 are being produced from the decay of ϕ^0 after the thermal freeze-out of ψ_1^0 . In this

²Here we have assumed other triplet fermions are heavier than ϕ^0 .

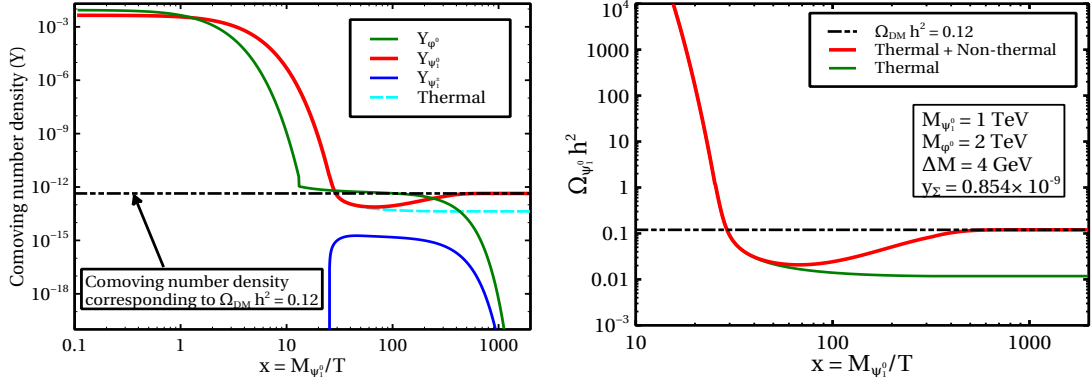


Figure 3. Left panel: Solution of coupled Boltzmann equations given in Eqs. (5.1)-(5.3) for a particular benchmark point $M_{\psi_1^0} = 1 \text{ TeV}$, $M_{\phi^0} = 2 \text{ TeV}$, $M_s = 200 \text{ GeV}$, $\Delta M = 4 \text{ GeV}$, $y_\Sigma = 0.854 \times 10^{-9}$ and $y_s = 1.5$. Right panel: Relic density of ψ_1^0 for thermal interactions ($y_\Sigma = 0$) and thermal plus non-thermal interactions ($y_\Sigma = 0.854 \times 10^{-9}$).

figure, the evolution of ψ_1^\pm is denoted by blue solid line, which gets produced from the decay of ϕ^0 at around $x \sim 25$ and eventually $Y_{\psi_1^\pm}$ becomes negligibly small after having a minute contribution to $Y_{\psi_1^0}$. This plot has been drawn for $M_{\psi_1^0} = 1 \text{ TeV}$, $M_{\phi^0} = 2 \text{ TeV}$, $M_s = 200 \text{ GeV}$, $\Delta M = M_{A^0} - M_{\phi^0} = M_{\phi^\pm} - M_{\phi^0} = 4 \text{ GeV}$ ³, $y_s = 1.5$ and $y_\Sigma = 0.854 \times 10^{-9}$ ⁴. In absence of any non-thermal contribution from the decay of ϕ^0 , the thermal abundance of ψ_1^0 is denoted by a cyan dashed line, which clearly shows the under abundance of ψ_1^0 for $M_{\psi_1^0} = 1 \text{ TeV}$ due to its large annihilations and co-annihilations. In the right panel of Fig. 3, we plot the variation of relic abundance of ψ_1^0 with x for the same benchmark point mentioned above. Here, the green solid line represents the relic abundance of ψ_1^0 due to thermal freeze-out only for $M_{\psi_1^0} = 1 \text{ TeV}$, i.e. the relic abundance of ψ_1^0 by considering its all possible annihilation and co-annihilation channels as shown in Fig. 2. From this figure it is clearly seen that for this benchmark point the thermal contribution, which is contributing only around $\sim 10\%$ of the canonical value $\Omega_{\text{DM}} h^2 = 0.12$, is not enough to reproduce the correct dark matter relic abundance. Hence there is need of an additional non-thermal contribution from the decay of ϕ^0 to compensate this deficit. Total abundance of ψ_1^0 including contributions from both thermal and non-thermal processes is shown by red solid line.

In Fig. 4 we show how $\Omega_{\psi_1^0} h^2$ varies with the mass of ψ_1^0 . In this plot, green dotted line is for the pure fermion triplet dark matter model [27] (discussed in Section 2) and it is clearly seen that in this model relic density of ψ_1^0 satisfies the Planck limit for $M_{\psi_1^0} \sim 2.2 \text{ TeV}$ which is consistent with the Ref. [27]. The blue dashed dotted line is for the present model without any non-thermal contribution to relic density i.e. Yukawa coupling $y_\Sigma = 0$. The difference between this case with the pure fermion triplet dark matter is that here we have extra annihilation and co-annihilation channels involving one or two S in the final states. In this case, we have chosen $M_s = 200 \text{ GeV}$ and $y_s = 1.5$. Hence, the relic density of ψ_1^0 for a particular mass $M_{\psi_1^0}$ is further suppressed. This is clearly evident from Fig. 4. Finally, the red solid line represents variation of dark matter relic density, which has both thermal as well as non-thermal contributions, for $\Delta M = 4 \text{ GeV}$, $M_{\phi^0} = 2 \text{ TeV}$, $M_s = 200 \text{ GeV}$, $y_\Sigma = 0.854 \times 10^{-9}$ and $y_s = 1.5$. Moreover, it also shows that for the chosen benchmark

³In this work, we have assumed $M_{\phi^\pm} = M_{A^0}$, which is possible if $\lambda_4 = \lambda_5$.

⁴For simplicity we have assumed Yukawa couplings $y_\Sigma^{11} = y_\Sigma^{21} = y_\Sigma^{31} = y_\Sigma$.

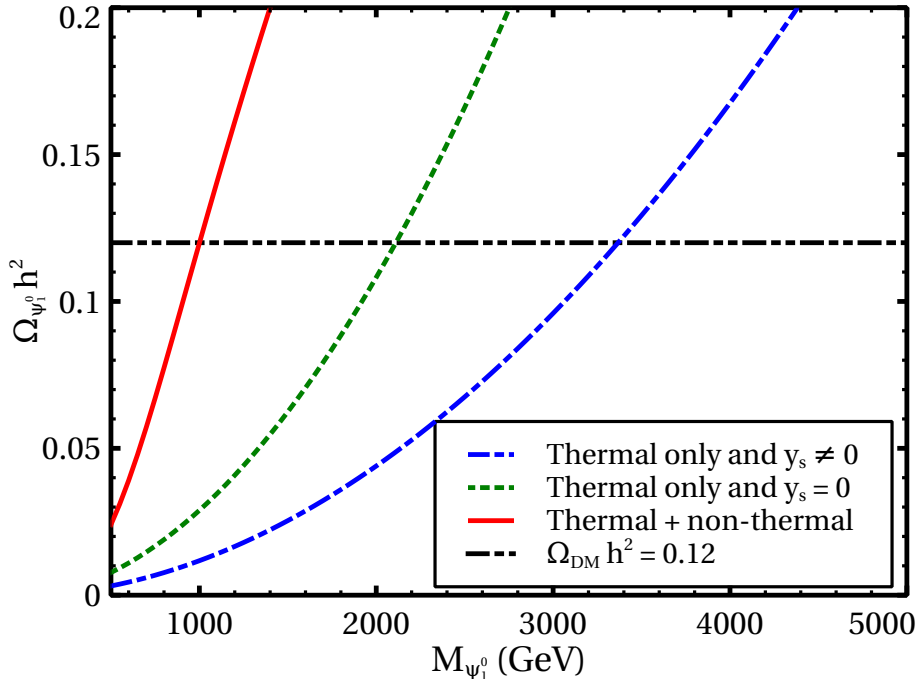


Figure 4. Variation of $\Omega_{\psi_1^0} h^2$ with $M_{\psi_1^0}$.

point the relic density of triplet fermion ψ_1^0 satisfies the Planck limit for a mass as low as $M_{\psi_1^0} = 1$ TeV. Please note that the plot shown in Fig. 4 is for illustrative purposes only in order to show the difference between possible scenarios discussed here. We have not taken non-perturbative effects into account in dark matter annihilations which can be significant if we go to high mass regime beyond 1 TeV. If we take them into account, as discussed by the authors of [28, 29], the point in the green and the blue lines where correct relic is satisfied will shift further towards right.

Now, we will present the effect of four model parameters on $Y_{\psi_1^0}$. These four model parameters have significant impacts on the non-thermal contributions to $Y_{\psi_1^0}$. While generating the four plots, we have kept fixed the other parameters (except the particular one which has been varied) to the same benchmark point we have used to generate Fig. 3. In Fig. 5(a), we show the variation of $Y_{\psi_1^0}$ with x for four different values of $\Delta M = M_{\phi^\pm} - M_{\phi^0} = M_{A^0} - M_{\phi^0}$. From this plot it is seen that the value of $Y_{\psi_1^0}$, after the thermal freeze-out of ψ_1^0 , increases as we decrease the mass splitting between ϕ^0 and other components of inert doublet Φ i.e. ϕ^\pm and A^0 ⁵. This can be understood as follows. From the inert doublet dark matter model [21, 45–50] we know that the abundance ϕ^0 increases as ΔM decreases and it is due to the cancellation between four point diagram and t, u channel diagrams for annihilation channels of ϕ^0 into gauge boson final states W^+W^-, ZZ and this is also true for the co-annihilation channels of inert scalars. Now, similarly here also Y_{ϕ^0} increases with decreasing ΔM . Again, from Eq. (5.1) one can easily notice that the non-thermal contribution to $Y_{\psi_1^0}$ coming from the decay of ϕ^0 is proportional to Y_{ϕ^0} . Hence $Y_{\psi_1^0}$ also increases as we decrease the mass splitting ΔM . The dependence of $Y_{\psi_1^0}$ on M_{ϕ^0} is shown in Fig. 5(b), where we have considered four different values of M_{ϕ^0} . From this plot, we see that $Y_{\psi_1^0}$ keeps on increasing as we

⁵In this work, for simplicity we choose $M_{\phi^\pm} = M_{A^0}$.

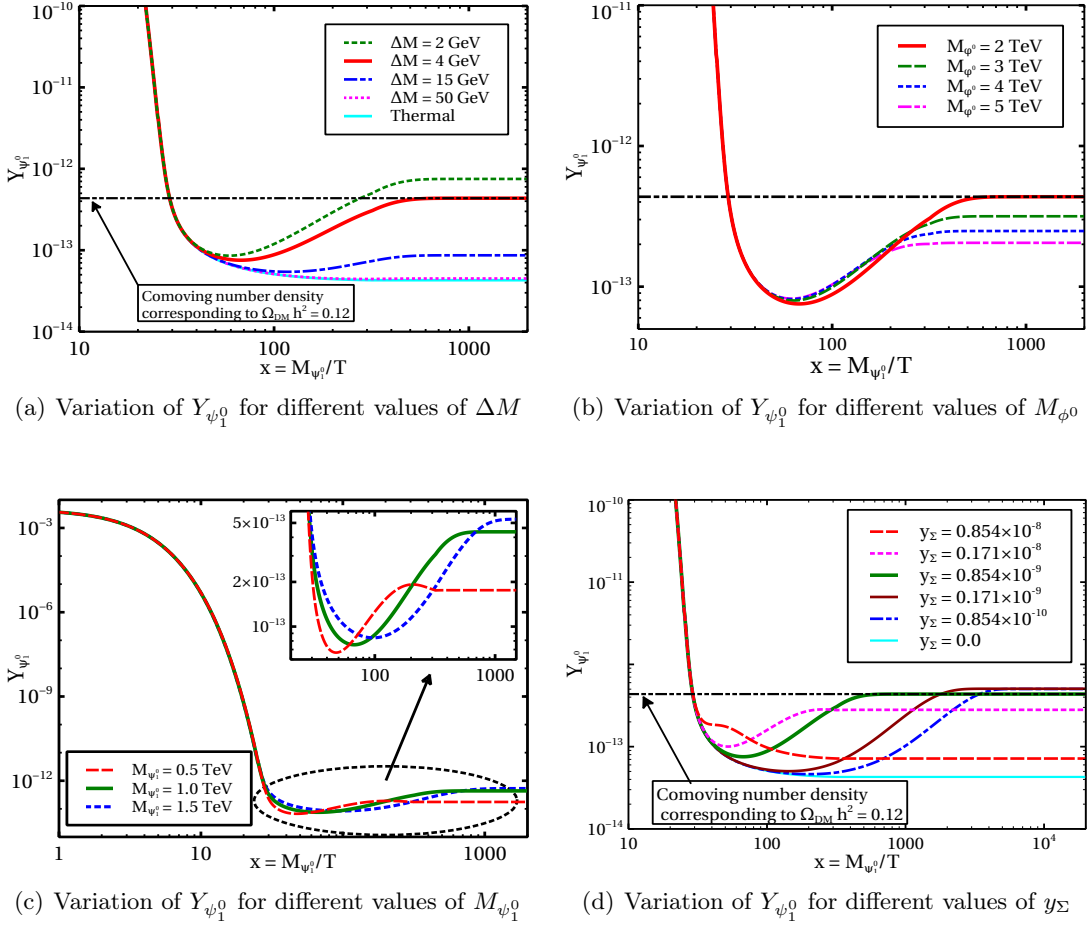


Figure 5. Comparison of $Y_{\psi_1^0}$ with respect to different model parameters.

lower the mass of ϕ^0 . This is due to the fact that the non-thermal contribution to $Y_{\psi_1^0}$ is proportional to two quantities. One is the abundance of ϕ^0 during the decay to ψ_1^0 , which occurs after the freeze-out of ϕ^0 (see left panel of Fig. 3) and other one is the corresponding decay width $\Gamma_{\phi^0 \rightarrow \psi_1^0}$. The behaviour of these two quantities are opposite with respect to M_{ϕ^0} . While decay width $\Gamma_{\phi^0 \rightarrow \psi_1^0}$ is proportional to M_{ϕ^0} , the comoving number density of ϕ^0 is less and becomes more suppressed for heavier ϕ^0 during the period when maximum decay to ψ_1^0 occurs. This is because, primarily the comoving number density of ϕ^0 after its freeze-out is less for higher value of M_{ϕ^0} (valid for a fixed value of ΔM and $M_{\phi^0} \gtrsim 1$ TeV) and additionally the total decay width $\Gamma_{\phi^0}^{\text{Total}}$ of ϕ^0 which gets enhanced with M_{ϕ^0} , has a negative impact on Y_{ϕ^0} (see Eq. (5.2)), which further reduces Y_{ϕ^0} with respect to M_{ϕ^0} in the considered range. Therefore, finally we get a combined effect of both the terms Y_{ϕ^0} and $\Gamma_{\phi^0 \rightarrow \psi_1^0}$ on $Y_{\psi_1^0}$, where $Y_{\psi_1^0}$ increases with decreasing M_{ϕ^0} . In Fig. 5(c), we demonstrate how $Y_{\psi_1^0}$ depends on the mass of ψ_1^0 . Here, we have shown the variation of $Y_{\psi_1^0}$ with x for three different values of $M_{\psi_1^0}$ such as 500 GeV, 1000 GeV and 1500 GeV. From this plot one can see that the final saturation value of $Y_{\psi_1^0}$ is more for dark matter candidate with heavier mass. This is due to the reason that the thermal abundance of ψ_1^0 , which is approximately inversely proportional to its annihilation and co-annihilation cross sections, is larger for heav-

ier ψ_1^0 . Also, we don't get same enhancement in $Y_{\psi_1^0}$ while going from 500 GeV to 1000 GeV and 1000 GeV to 1500 GeV. This is because, the decay width $\Gamma_{\phi^0 \rightarrow \psi_1^0}$ becomes phase space suppressed as $M_{\psi_1^0} \rightarrow M_{\phi^0}$. As a result, non-thermal contribution, which is proportional to $\Gamma_{\phi^0 \rightarrow \psi_1^0}$, decreases with $M_{\psi_1^0}$. Hence, we get the saturation values of $Y_{\psi_1^0}$ for 1000 GeV and 1500 GeV, which are not much different from each other. Finally, we show the dependence of the evolution of $Y_{\psi_1^0}$ with x on Yukawa coupling y_Σ , where we have considered six different values for the Yukawa coupling y_Σ and we find that the correct relic density is achieved for $y_\Sigma = 0.854 \times 10^{-9}$. As the total decay width $\Gamma_{\phi^0}^{\text{Total}}$ of ϕ^0 is proportional to y_Σ^2 , the smaller y_Σ results in a late decay of ϕ^0 to ψ_1^0 . Hence, the increase of $Y_{\psi_1^0}$ due to the non-thermal decay of $\phi^0 \rightarrow \psi_1^0 + \nu$ also occurs much later for smaller value of y_Σ . This effect can be understood by comparing the magenta dashed curve and blue dashed-dotted curve in Fig. 5(d), where magenta and blue lines are for $y_\Sigma = 0.171 \times 10^{-8}$ and 0.854×10^{-10} respectively. Further, we have seen an anomalous behaviour in the effect of Yukawa coupling y_Σ on $Y_{\psi_1^0}$. Generally for the non-thermal dark matter (FIMP), the relic abundance increases as we increase the coupling between mother particle and dark matter. As a result, more dark matter particles are produced from the decay of mother particle which is assumed to be in thermal equilibrium and the equilibrium abundance of mother particle does not depend on its decay width to FIMP dark matter. However, in the present case the mother particle ϕ^0 becomes out of thermal equilibrium at the time of non-thermal production of ψ_1^0 . Now, from the Boltzmann equation of ψ_1^0 (Eq. (5.1)), one can easily see that the rate of increase of $Y_{\psi_1^0}$ due to the decay to ϕ^0 is proportional to Y_{ϕ^0} and $\Gamma_{\phi^0 \rightarrow \psi_1^0}$. The comoving number density Y_{ϕ^0} can be obtained by solving the Boltzmann equation for ϕ^0 (Eq. (5.2)), where the last term proportional to the total decay width of ϕ^0 ($\Gamma_{\phi^0}^{\text{Total}}$) further decreases Y_{ϕ^0} from its freeze-out abundance. Now, if we increase the Yukawa coupling y_Σ , the total decay width $\Gamma_{\phi^0}^{\text{Total}}$ which is proportional to y_Σ^2 , also increases. This in turn decreases Y_{ϕ^0} . On the other hand, any increase of y_Σ is also accompanied by an enhancement of the decay width $\Gamma_{\phi^0 \rightarrow \psi_1^0}$. Therefore, in the Boltzmann equation of ψ_1^0 , there is a competition between the two quantities Y_{ϕ^0} and $\Gamma_{\phi^0 \rightarrow \psi_1^0}$, which are behaving oppositely with respect to the variation of y_Σ . The final abundance of ψ_1^0 will follow the behaviour of that quantity which depends more strongly on y_Σ . From Fig. 5(d), we find that the final abundance of ψ_1^0 actually decreases as we increase the Yukawa coupling y_Σ from 0.171×10^{-10} to 0.854×10^{-8} . This makes the present scenario different from the usual FIMP scenario [12, 51–53], where the final abundance of dark matter always increases with associated couplings.

In Fig. 6, we show our allowed parameter space in $y_\Sigma - \Delta M$ plane which reproduces the correct dark matter relic density. The colour code is indicating the mass of our dark matter ψ_1^0 which we have varied between 500 GeV to 1500 GeV while the corresponding mass of ϕ^0 is scanned over the following range: $2 M_{\psi_1^0} \leq M_{\phi^0} \leq 2 M_{\psi_1^0} + 2000$ GeV. The plot in left panel is for a fixed value of other Yukawa coupling y_s which we have kept fixed at 1.5 while for the plot in the right panel, we have varied the Yukawa coupling y_s between 0.1 to 2. From the plot in the left panel, one can see that to produce the dark matter relic density in the right ballpark, we need $10^{-10} \leq y_\Sigma \leq 4 \times 10^{-9}$ depending upon the mass splitting ΔM between the inert scalars, which is also tightly constrained to be less than 5.5 GeV. However, from the right panel it is also noticeable that these ranges of Yukawa coupling y_Σ and mass splitting ΔM are slightly larger when we have also varied the singlet Yukawa coupling $0.1 \leq y_s \leq 2$. This is because the thermal contribution to relic density becomes fixed for a particular set of values of $M_{\psi_1^0}$, M_{ϕ^0} , M_s , ΔM and y_s . In this case, the amount of

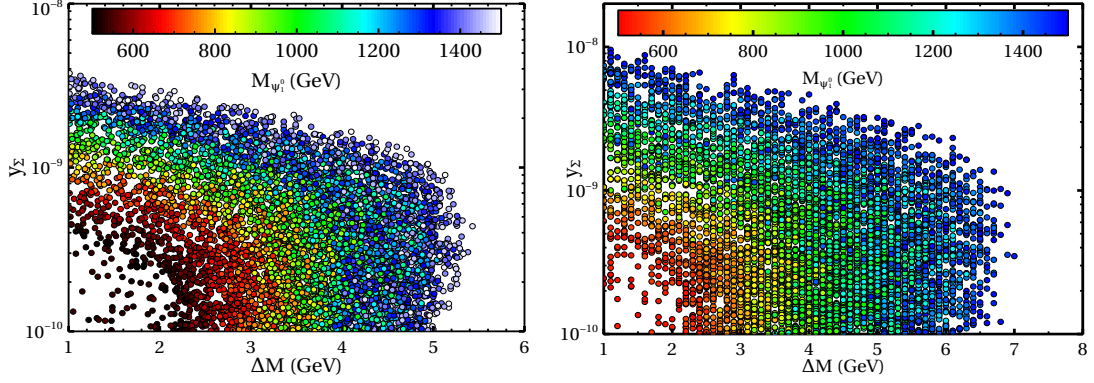


Figure 6. Allowed parameter space in $y_\Sigma - \Delta M$ for $y_s = 1.5$ (left panel) and $0.1 \leq y_s \leq 2.0$ (right panel). In both plots mass of ϕ^0 has been varied between 1 TeV to 5 TeV and M_s is kept fixed at 200 GeV.

deficit in relic density which is compensated by the non-thermal production is also a definite number as the total relic density should lie with the observed band $0.1166 \leq \Omega_{\text{DM}} h^2 \leq 0.1206$ in 68% C.L. However, if we vary the singlet Yukawa y_s while keeping others fixed at their respective values (ΔM , M_ϕ , $M_{\psi_1^0}$ and M_s) then the thermal contribution to $\Omega_{\psi_1^0} h^2$ also varies and hence we require different non-thermal contributions to achieve correct dark matter relic density and consequently more parameter space in $y_\Sigma - \Delta M$ plane become allowed. Later when we will discuss the constraints coming from the indirect detection we will see that for the considered mass range of $M_{\psi_1^0}$ we need $y_s \gtrsim 1$ (see Fig. 10). Moreover, from both these plots it is clearly evident that for heavier dark matter mass we need larger values of y_Σ and ΔM to achieve $\Omega_{\psi_1^0} h^2$ in the correct ballpark.

6 LHC constraints on ψ_1^\pm

In this section, we briefly discuss the testability of our model at the LHC experiment. There have been several dedicated searches for possible dark matter signatures at colliders, a recent summary of which can be found in [54, 55]. Instead of usual missing transverse energy associated with dark matter production at colliders, in our model there exists a different (rather unique to a limited class of scenarios) signature that is within the reach of LHC. This is basically the collider production of different components of the fermion triplet Σ_{1R} through gauge interactions and subsequent decay of the heavier components into the lighter one. Since dark matter candidate ψ_1^0 is the lightest component, the heavier component ψ_1^\pm must decay into ψ_1^0 and other SM particles. This decay is actually interesting due to small mass splitting $\Delta M_{\text{triplet}} \simeq 166$ MeV between $M_{\psi_1^\pm}$ and $M_{\psi_1^0}$ for $M_\Sigma \gtrsim 1$ TeV. For such a small mass difference, the dominant decay mode is $\psi_1^\pm \rightarrow \psi_1^0 \pi^\pm$, the corresponding decay width of which is given by Eq. (5.4). Such tiny decay width keeps the lifetime of ψ_1^\pm considerably long enough that it can reach the detector before decaying. In fact, the ATLAS experiment at the LHC has already searched for such long-lived charged particles with lifetime ranging from 10 ps to 10 ns, with maximum sensitivity around 1 ns [56]. In the decay $\psi_1^\pm \rightarrow \psi_1^0 \pi^\pm$, the final state pion typically has very low momentum and it is not reconstructed in the detector. On the other hand the dark matter particle in the final state ψ_1^0 is perfectly stable and leaves the detector without interacting. Therefore, it gives rise to a signature where a charged particle

leaves a track in the inner parts of the detector and then disappears leaving no tracks in the portions of the detector at higher radii. The ATLAS constraints on such disappearing charged track signatures for a long lived chargino decaying into a pion and wino dark matter is shown as the solid green line in Fig. 7. Since our dark matter multiplet is similar to the multiplet containing chargino, wino with similar production cross section at LHC as shown in Table 1 for fermion triplets and in [57, 58] for gauginos, we compare our model predictions against this constraint from ATLAS. The lifetime predictions for ψ_1^\pm as a function of DM mass is shown as the solid red line in Fig. 7. It can be seen that the existing LHC constraint can already rule out DM masses below 500 GeV from its searches for disappearing charged tracks, keeping the DM parameter space considered in this study within near future sensitivity.

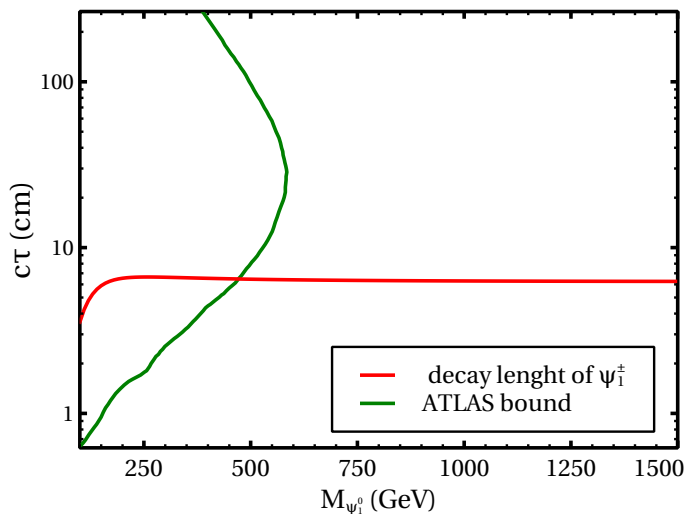


Figure 7. Lifetime of ψ_1^\pm versus DM mass compared with the ATLAS bound on disappearing charge track searches.

$M_{\psi_1^0}$ (TeV)	$\sigma_{pp \rightarrow \psi_1^+ \psi_1^-}$ (pb)	$\sigma_{pp \rightarrow \psi_1^\pm \psi_1^0}$ (pb)
0.5	1.493×10^{-2}	4.394×10^{-2}
0.6	6.338×10^{-3}	1.92×10^{-2}
0.7	2.938×10^{-3}	9.1×10^{-3}
0.8	1.464×10^{-3}	4.6×10^{-3}
0.9	7.588×10^{-4}	2.43×10^{-3}
1.0	4.103×10^{-4}	1.33×10^{-3}
1.1	2.305×10^{-4}	7.468×10^{-4}
1.2	1.305×10^{-4}	4.308×10^{-4}
1.3	7.600×10^{-5}	2.508×10^{-4}
1.4	4.490×10^{-5}	1.494×10^{-4}
1.5	2.687×10^{-5}	8.978×10^{-5}

Table 1. Production cross sections of $\psi_1^+ \psi_1^-$ and $\psi_1^\pm \psi_1^0$ from pp collisions at $\sqrt{s} = 14$ TeV LHC.

7 Direct Detection

The most convincing way to probe a particle dark matter candidate is the direct detection experiments. There have been serious efforts in this direction for last few decades where ground based detectors made up of different heavy nuclei have been used to probe processes where a DM particle passing through the detector can interact with a nuclei giving rise to some recoil. Such experiments have significantly improved their sensitivities over the years, with their present exclusion limits on spin independent DM-nucleon scattering cross section lying very close to the coherent neutrino-nucleon scattering rate [6–10]. Interestingly, our present model has good prospects for direct detection frontiers which is usually not there for purely freeze-in type dark matter candidates. Being part of an electroweak multiplet, the dark matter can interact with SM through gauge interactions and also through scalar interactions present due to the singlet scalar field S' . Due to the absence of neutral current interactions of our dark matter candidate at tree level, the gauge boson mediated DM-nucleon scattering can arise only at radiative level. However, due to the existence of singlet scalar mixing with the SM like Higgs, such scalar mediated DM-nucleon scattering can occur at tree level as well. The Feynman diagrams corresponding to these processes are shown in Fig. 8 all of which can lead to spin independent (SI) direct detection (DD) scattering processes. For pure triplet fermion case we have to exclude the last one as there exists no singlet scalar in that scenario. The dark matter candidate ψ_1^0 has two different one loop DD scattering: a Higgs penguin with W^\pm loop and the box diagram in Fig. 8. The low energy effective Lagrangian for the ψ_1^0 -quark one loop interaction have already been discussed in [59]. So the effective Lagrangian for the loop diagrams can be written as

$$\mathcal{L}_{\psi_1^0 q} = \sum_i \lambda_q^i \bar{\psi}_1^0 \psi_1^0 \bar{q} q \quad (7.1)$$

$$\begin{aligned} \lambda_q^i = & -\alpha_2^2 \frac{m_{q_i}}{m_{\psi_1^0} m_h^2} \frac{1 - 4\eta_W + 3\eta_W^2 + (2 - 4\eta_W) \log \eta_W}{(1 - \eta_W)^3} \\ & + \alpha_2^2 \frac{m_{q_i}}{m_{\psi_1^0} m_W^2} \frac{2 - 3\eta_W + 6\eta_W^2 - 5\eta_W^3 + 3\eta_W(1 + \eta_W^2) \log \eta_W}{6(1 - \eta_W)^4} \end{aligned} \quad (7.2)$$

where $\eta_W \equiv \frac{m_W^2}{m_{\psi_1^0}^2}$ and $\alpha_2 = \frac{g^2}{4\pi}$. In Eq. (7.2), the first term is the effective coupling for the Higgs penguin diagram and the second term is the same for the box diagram. We have shown the corresponding spin-independent direct detection cross-section as a function of DM mass in the left panel of Fig. 9, which is about two orders of magnitude below the current XENON1T bound [8]. In spite of electroweak gauge interactions being involved in the scattering, this is in a way expected due to loop suppressions involved.

The other possible diagram coming from the introduction of the singlet scalar can, on the other hand, give rise to larger DD cross-section if the singlet scalar S' has sizeable mixing with the SM like Higgs. The relevant cross section can be written as

$$\sigma_{\text{SI}} = \frac{y_s^2 \mu_{\psi_1^0 n}^2 m_n^2}{\pi m_s^4 v^2} f_p^2 \xi^2 \quad (7.3)$$

where y_s , f_p , ξ and m_n are the new Yukawa coupling, form factor, S' -Higgs mixing parameter (defined in Eq. (3.8)), and nucleon mass respectively. We have also fixed the singlet mass

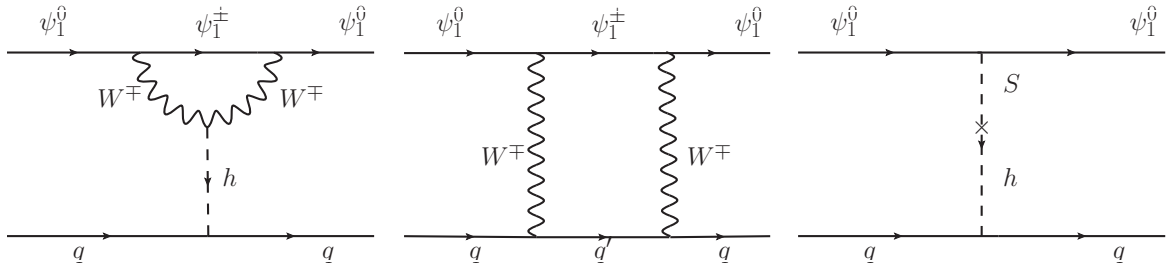


Figure 8. Spin-independent DD scattering processes in the model. The first two processes are for pure triplet fermion dark matter model while the last one arises additionally in the present model due to the introduction of the singlet scalar S' .

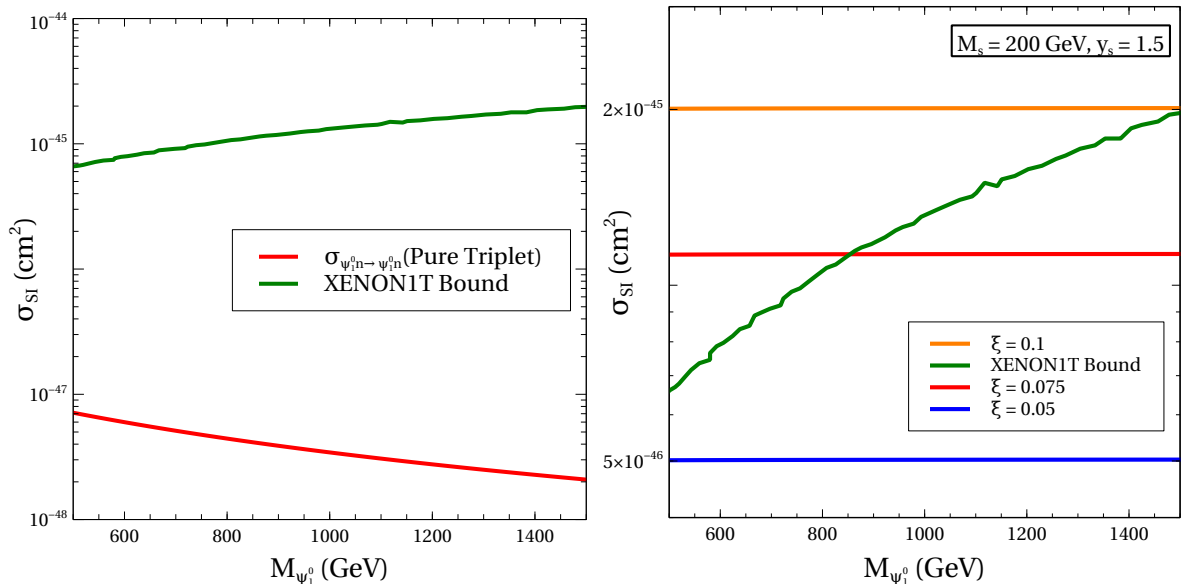


Figure 9. Left panel: DD cross-section for pure triplet fermion as a functions of DM mass. Right panel: DD cross-section for singlet scalar mediated diagram as a function of DM mass for different benchmark values of ξ with fixed $M_s = 200$ GeV and $y_s = 1.5$.

(M_s) at 200 GeV, like in the calculation for relic abundance. As the DM-nucleon reduced mass $\mu_{\psi_1^0 n}$ is nearly close to the mass of the nucleon for the chosen range of DM masses, this scattering cross section is almost independent of the DM mass. This in fact serves as another motivation of introducing the singlet scalar S' apart from being responsible for generating DM mass dynamically. This singlet scalar allows the model to be testable at ongoing and upcoming direct detection experiments for a wide range of DM masses. We show the contribution of this scalar mediated diagram to DD scattering in the right panel of Fig. 9 for three different mixing parameter ξ values ($\xi = 0.1, 0.075, 0.05$). From the Fig. 9 it is clear that the σ_{SI} lies above the XENON1T bound for $\xi = 0.1$, whereas for $\xi = 0.075$ it is partially allowed and for $\xi = 0.05$ it is just below the present bound for the chosen mass range of DM.

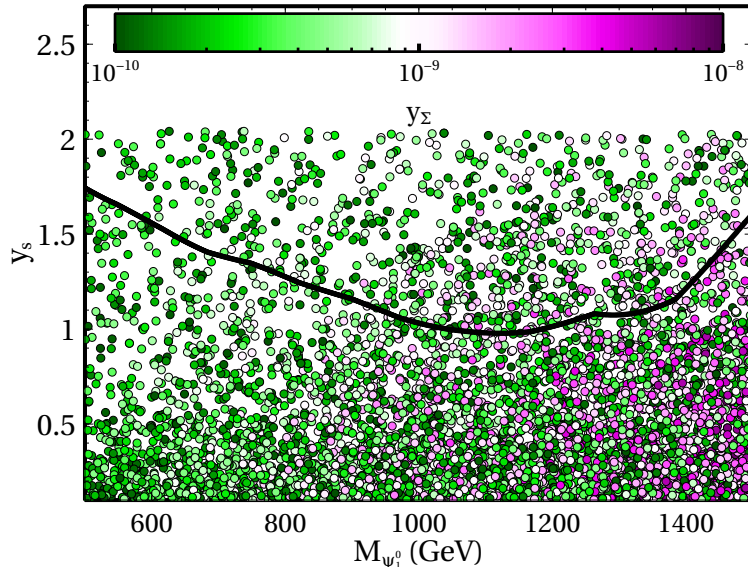


Figure 10. Parameter space of Yukawa coupling y_s and $M_{\psi_1^0}$ that satisfy the relic density constraint. The color-bar indicates the variation of the another Yukawa y_{Σ} . The Black line corresponds to the Fermi-LAT bound, the points above that line are allowed. To generate this plot we have fixed the singlet mass (M_s) at 200 GeV.

8 Indirect Detection

Apart from direct detection experiments, DM parameter space in our model can also be probed at different indirect detection experiments (space as well as ground based) that are looking for SM particles produced either through DM annihilations or via DM decay in the local Universe. Among these final states, photon and neutrinos, being neutral and stable can reach the indirect detection experiments without getting affected much by intermediate regions. If the DM is of the type we have in our model, having TeV scale masses and sizeable interaction with the SM particles, these photons lie in the gamma ray regime that can be measured at space based telescopes like the Fermi-LAT or ground based telescopes like MAGIC. Here we constrain the DM parameter space from the indirect detection bounds arising from the global analysis of the Fermi-LAT and MAGIC observations of dSphs [39].

Since the heavier components of the fermion triplet are not there in the present Universe, we need to consider the DM self annihilations into the charged particles of the SM. The only possible process of this type is the DM annihilation into a pair of W bosons which is indeed constrained tightly from gamma ray observations [39]. Such bounds on $\langle\sigma v\rangle_{\text{DMDM}\rightarrow W+W^-}$ are derived assuming 100% annihilation of DM into these final states. Since we have another DM annihilation in this model namely, the one with a pair of singlet scalars S' in the final states which do not contribute to gamma rays due to neutral final states, we take into account the relative factor between these two annihilation rates while applying the indirect detection bound on $\langle\sigma v\rangle_{\text{DMDM}\rightarrow W+W^-}$. Due to sizeable DM annihilation rates into neutral singlet scalars in our model, the gamma ray constraints on DM annihilations into W boson pairs get weaker in our model, saving the parameter space under study. It should be noted that in the pure fermion triplet dark matter model, gamma ray bound will completely rule out low mass region of DM mass we are studying [28] as the annihilation rate for $\langle\sigma v\rangle_{\text{DMDM}\rightarrow W+W^-}$ is 100% in that model. Therefore, weakening the indirect detection bound arise as another motivation

for the singlet scalar S' apart from generating DM mass dynamically and giving rise to tree level direct detection rates as discussed before. In Fig. 10 we have shown allowed parameter space in the y_s versus $M_{\psi_1^0}$ plane where we have also varied Yukawa of the inert doublet y_Σ while fixing the singlet scalar mass at 200 GeV. All the points shown there are satisfying the relic density constraint and the black solid line corresponds to the present Fermi-LAT plus MAGIC bound on DM annihilation to W^\pm . The points below the black line are ruled out from these bounds which shows that we need large y_s to satisfy the present bound. As the x-axis goes all the way upto DM mass of 1.5 TeV where non-perturbative effects (Sommerfeld enhancement) on DM annihilations can be sizeable, we use the results of [28] to derive the exclusion line shown in Fig. 10. As we go into higher mass values, the Sommerfeld enhancement becomes more and more efficient which can be seen by the sharp rise in the black solid line towards the right end of the plot, requiring stronger Yukawa coupling y_s to keep the DM self annihilations to neutral particles more dominant over $\langle\sigma v\rangle_{\text{DMDM}\rightarrow\text{W}+\text{W}^-}$. Future data from gamma ray telescopes should be able to probe more parts of this region of dark matter masses as well as Yukawa coupling y_s , keeping the indirect detection prospects of the model very promising.

9 Summary and Conclusion

We have studied a minimal model for dark matter and radiative neutrino mass where dark matter relic abundance is generated from a hybrid setup consisting of both freeze-out and freeze-in scenarios. Considering a radiative type III seesaw scenario with the lightest fermion triplet being the dark matter candidate stabilised by an in built \mathbb{Z}_2 symmetry, we first show how the neutral component of this fermion triplet having mass around 1 TeV remains under-abundant from thermal freeze-out mechanism. We then consider a non-thermal (freeze-in) contribution from the late decay of \mathbb{Z}_2 -odd scalar doublet to fill the deficit created during thermal freeze-out. We solve the coupled Boltzmann equations involving the mother particles and the dark matter candidate and find the parameter space that can lead to the correct relic abundance of dark matter. Due to the coupled nature of these equations, we can simultaneously constrain both dark matter as well as mother particle parameter space. The mother particle, being heavy, freezes out first followed by the freeze-out of dark matter and then the late decay of the mother particle into the dark matter particles. Such a hybrid setup has some interesting differences from the usual freeze-in dark matter scenarios. One notable difference we found was the dependence of non-thermal contribution on the corresponding Yukawa coupling between mother particle and dark matter. In the usual FIMP scenario, the non-thermal contribution always increases with such Yukawa, while in the present case it is not necessarily so. This is due to the role of the same Yukawa coupling in deciding the freeze-out abundance of the mother particle which later gets converted into non-thermal part of DM through late decay.

Apart from satisfying the correct relic abundance of dark matter within this hybrid setup having distinguishable features from pure WIMP and pure FIMP scenarios, the model also has promising detection prospects at collider, direct and indirect detection experiments. The presence of a scalar singlet which generates the dark matter mass dynamically in this model, plays a non-trivial role in keeping the model parameter space not only allowed from current experimental constraints but also very close to present as well as upcoming experimental sensitivity leaving a very promising scope for verifiability. This is in contrast to the typical freeze-in dark matter models which have very limited detection prospects due to tiny

couplings. In principle, any mass of dark matter in the thermally under-abundant regime ($M_{\psi_1^0} \leq 2.2$ TeV) can be revived by adding a non-thermal contribution. However, due to tight constraints from LHC (evident from Fig. 7), we get a lower bound of around 500 GeV. Also, as we go above 1 TeV mass, the indirect detection constraints become severe (evident from Fig. 10), requiring large couplings of dark with the singlet scalar. Such large couplings will get large corrections under renormalisation group evolutions, making the model non-perturbative at a low scale. Therefore we stick to a mass window near the 1 TeV.

In the neutrino sector also this model remains predictive as the lightest neutrino mass is vanishingly small due to tiny Yukawa couplings of the lightest fermion triplet, required for its non-thermal production at late epochs. Such vanishing lightest neutrino mass can have interesting consequences at experiments sensitive to the absolute neutrino mass scale. The model however suffers from the fine-tuning issue related to the above mentioned Yukawa coupling of the lightest fermion triplet to the leptons. Such tiny couplings can be generated within the framework of more general scenarios some of which also provide a UV completion [53, 60, 61].

Acknowledgments

One of the authors AB would like to acknowledge financial support from SERB, Govt. of INDIA through NPDF fellowship under the project id. PDF/2017/000490. He also thanks Alexander Pukhov for a few email conversation regarding package micrOMEGAs. Moreover, AB gratefully acknowledges the cluster computing facility at Harish-Chandra Research Institute, Allahabad (<http://www.hri.res.in/cluster/>). AB and DN would like to thank Amit Dutta Banik for various discussions. DB acknowledges the support from IIT Guwahati start-up grant (reference number: xPHYSUGIITG01152xxDB001) and Associateship Programme of IUCAA, Pune. He also acknowledges the hospitality and facilities provided by School of Liberal Arts, Seoul-Tech, Seoul 139-743, Korea where part of this work was completed.

A Full calculation of the Lagrangian of fermionic triplet Σ

We have constructed a fermionic triplet Σ using Σ_R and its CP conjugate $\Sigma_R^c = C \overline{\Sigma_R}^T$ as $\Sigma = \Sigma_R + \Sigma_R^c$. The Lagrangian of Σ can be written as

$$\mathcal{L}_{triplet} = \frac{i}{2} \text{Tr}[\overline{\Sigma} \not{D} \Sigma] - \frac{1}{2} \text{Tr}[\overline{\Sigma} M_\Sigma \Sigma], \quad (\text{A.1})$$

$$= \frac{i}{2} \text{Tr}[\overline{\Sigma_R} \not{D} \Sigma_R] + \frac{i}{2} \text{Tr}[\overline{\Sigma_R^c} \not{D} \Sigma_R^c] - \left(\frac{1}{2} \text{Tr}[\overline{\Sigma_R^c} M_\Sigma \Sigma_R] + h.c. \right). \quad (\text{A.2})$$

The covariant derivative of Σ_R is defined as

$$D_\mu \Sigma_R = \partial_\mu \Sigma_R + i g \left[\sum_{a=1}^3 \frac{\sigma^a}{2} W_\mu^a, \Sigma_R \right], \quad (\text{A.3})$$

where, g is the $SU(2)_L$ gauge coupling and W_μ^a ($a = 1$ to 3) are three corresponding gauge bosons. Now, using the expression of Σ_R given in Eq. (2.1), the covariant derivative of Σ_R can be further expressed in terms of the components of Σ_R as

$$D_\mu \Sigma_R = \partial_\mu \Sigma_R + \frac{i g}{2} \begin{pmatrix} \sqrt{2}(W_\mu^+ \Sigma_R^- - W_\mu^- \Sigma_R^+) & 2(W_\mu^3 \Sigma_R^+ - W_\mu^+ \Sigma_R^0) \\ 2(W_\mu^- \Sigma_R^0 - W_\mu^3 \Sigma_R^-) & \sqrt{2}(W_\mu^- \Sigma_R^+ - W_\mu^+ \Sigma_R^-) \end{pmatrix}. \quad (\text{A.4})$$

Moreover, using Eq. (2.1) and the definition of Σ_R^c , the CP conjugate of Σ_R can also be expressed in a 2×2 matrix notation as

$$\Sigma_R^c = \begin{pmatrix} \Sigma_R^{0^c}/\sqrt{2} & \Sigma_R^{-c} \\ \Sigma_R^{+c} & -\Sigma_R^{0^c}/\sqrt{2} \end{pmatrix}, \quad (\text{A.5})$$

Similarly, using Eq. (A.3) and Eq. (A.5), the covariant derivative of Σ_R^c is given by

$$D_\mu \Sigma_R^c = \partial_\mu \Sigma_R^c + \frac{ig}{2} \begin{pmatrix} \sqrt{2}(W_\mu^+ \Sigma_R^{+c} - W_\mu^- \Sigma_R^{-c}) & 2(W_\mu^3 \Sigma_R^{-c} - W_\mu^+ \Sigma_R^{0^c}) \\ 2(W_\mu^- \Sigma_R^{0^c} - W_\mu^3 \Sigma_R^{+c}) & \sqrt{2}(W_\mu^- \Sigma_R^{-c} - W_\mu^+ \Sigma_R^{+c}) \end{pmatrix}. \quad (\text{A.6})$$

Now, using Eq. (A.4), let us simplify the first term of Eq. (A.2):

$$\begin{aligned} & \frac{i}{2} \text{Tr}[\overline{\Sigma}_R \not{D} \Sigma_R] \\ &= \frac{i}{2} \left(\overline{\Sigma}_R^0 \not{\partial} \Sigma_R^0 + \overline{\Sigma}_R^- \not{\partial} \Sigma_R^- + \overline{\Sigma}_R^+ \not{\partial} \Sigma_R^+ \right) - \frac{g}{4} \left(2 \overline{\Sigma}_R^0 \gamma^\mu \Sigma_R^- W_\mu^+ - 2 \overline{\Sigma}_R^0 \gamma^\mu \Sigma_R^+ W_\mu^- \right. \\ & \quad \left. + 2 \overline{\Sigma}_R^- \gamma^\mu \Sigma_R^0 W_\mu^- - 2 \overline{\Sigma}_R^+ \gamma^\mu \Sigma_R^0 W_\mu^+ + 2 \overline{\Sigma}_R^+ \gamma^\mu \Sigma_R^+ W_\mu^3 - 2 \overline{\Sigma}_R^- \gamma^\mu \Sigma_R^- W_\mu^3 \right). \quad (\text{A.7}) \end{aligned}$$

Moreover, using the relations $\Sigma_R^{+c} = C \overline{\Sigma}_R^{+T}$ and $\Sigma_R^{0^c} = C \overline{\Sigma}_R^{0T}$, one can further rewrite the above equation in terms of Σ_R^{+c} instead of Σ_R^+ as

$$\begin{aligned} & \frac{i}{2} \text{Tr}[\overline{\Sigma}_R \not{D} \Sigma_R] \\ &= \frac{i}{2} \left(\overline{\Sigma}_R^0 \not{\partial} \Sigma_R^0 + \overline{\Sigma}_R^- \not{\partial} \Sigma_R^- + \overline{\Sigma}_R^{+c} \not{\partial} \Sigma_R^{+c} \right) - \frac{g}{4} \left(2 \overline{\Sigma}_R^0 \gamma^\mu \Sigma_R^- W_\mu^+ + 2 \overline{\Sigma}_R^{+c} \gamma^\mu \Sigma_R^{0^c} W_\mu^- \right. \\ & \quad \left. + 2 \overline{\Sigma}_R^- \gamma^\mu \Sigma_R^0 W_\mu^- + 2 \overline{\Sigma}_R^{0^c} \gamma^\mu \Sigma_R^{+c} W_\mu^+ - 2 \overline{\Sigma}_R^{+c} \gamma^\mu \Sigma_R^+ W_\mu^3 - 2 \overline{\Sigma}_R^- \gamma^\mu \Sigma_R^- W_\mu^3 \right). \quad (\text{A.8}) \end{aligned}$$

In the above equation, we have used the following properties of charge conjugation operator:

$$\begin{aligned} C^{-1} \gamma_\mu C &= -\gamma_\mu^T, \\ C^{-1} \gamma_5 C &= \gamma_5^T, \\ C^T &= -C, \\ C^\dagger &= C^{-1}. \end{aligned} \quad (\text{A.9})$$

Similarly, let us simplify the second term of Eq. (A.2) using Eq. (A.6):

$$\begin{aligned} & \frac{i}{2} \text{Tr}[\overline{\Sigma}_R^c \not{D} \Sigma_R^c] \\ &= \frac{i}{2} \left(\overline{\Sigma}_R^{0^c} \not{\partial} \Sigma_R^{0^c} + \overline{\Sigma}_R^{-c} \not{\partial} \Sigma_R^{-c} + \overline{\Sigma}_R^{+c} \not{\partial} \Sigma_R^{+c} \right) - \frac{g}{4} \left(2 \overline{\Sigma}_R^{0^c} \gamma^\mu \Sigma_R^{+c} W_\mu^+ - 2 \overline{\Sigma}_R^{0^c} \gamma^\mu \Sigma_R^{-c} W_\mu^- \right. \\ & \quad \left. + 2 \overline{\Sigma}_R^{+c} \gamma^\mu \Sigma_R^{0^c} W_\mu^- - 2 \overline{\Sigma}_R^{-c} \gamma^\mu \Sigma_R^{0^c} W_\mu^+ + 2 \overline{\Sigma}_R^{-c} \gamma^\mu \Sigma_R^{-c} W_\mu^3 - 2 \overline{\Sigma}_R^{+c} \gamma^\mu \Sigma_R^{+c} W_\mu^3 \right). \quad (\text{A.10}) \end{aligned}$$

One can change the field Σ_R^{-c} by Σ_R^- in the above equation using the relation $\Sigma_R^{-c} = C \overline{\Sigma}_R^{-T}$ and the properties of C operator mentioned in Eq. (A.9) as

$$\begin{aligned} & \frac{i}{2} \text{Tr}[\overline{\Sigma}_R^c \not{D} \Sigma_R^c] \\ &= \frac{i}{2} \left(\overline{\Sigma}_R^{0^c} \not{\partial} \Sigma_R^{0^c} + \overline{\Sigma}_R^- \not{\partial} \Sigma_R^- + \overline{\Sigma}_R^{+c} \not{\partial} \Sigma_R^{+c} \right) - \frac{g}{4} \left(2 \overline{\Sigma}_R^{0^c} \gamma^\mu \Sigma_R^{+c} W_\mu^+ + 2 \overline{\Sigma}_R^- \gamma^\mu \Sigma_R^0 W_\mu^- \right. \\ & \quad \left. + 2 \overline{\Sigma}_R^{+c} \gamma^\mu \Sigma_R^{0^c} W_\mu^- + 2 \overline{\Sigma}_R^0 \gamma^\mu \Sigma_R^- W_\mu^+ - 2 \overline{\Sigma}_R^- \gamma^\mu \Sigma_R^- W_\mu^3 - 2 \overline{\Sigma}_R^{+c} \gamma^\mu \Sigma_R^{+c} W_\mu^3 \right). \quad (\text{A.11}) \end{aligned}$$

Now, adding Eq. (A.8) and Eq. (A.11), we get

$$\begin{aligned}
& \frac{i}{2} \text{Tr}[\overline{\Sigma}_R \not{D} \Sigma_R] + \frac{i}{2} \text{Tr}[\overline{\Sigma}_R^c \not{D} \Sigma_R^c], \\
&= \frac{i}{2} \left(\overline{\Sigma}_R^0 \not{\partial} \Sigma_R^0 + \overline{\Sigma}_R^{0c} \not{\partial} \Sigma_R^{0c} \right) + i \left(\overline{\Sigma}_R^- \not{\partial} \Sigma_R^- + \overline{\Sigma}_R^{+c} \not{\partial} \Sigma_R^{+c} \right) - g \left(\overline{\Sigma}_R^- \gamma^\mu \Sigma_R^0 W_\mu^- + \overline{\Sigma}_R^{+c} \gamma^\mu \Sigma_R^{0c} W_\mu^- \right. \\
&\quad \left. + \overline{\Sigma}_R^0 \gamma^\mu \Sigma_R^- W_\mu^+ + \overline{\Sigma}_R^{0c} \gamma^\mu \Sigma_R^{+c} W_\mu^+ - \overline{\Sigma}_R^{+c} \gamma^\mu \Sigma_R^+ W_\mu^3 - \overline{\Sigma}_R^- \gamma^\mu \Sigma_R^- W_\mu^3 \right). \tag{A.12}
\end{aligned}$$

Let us define two fermionic state as

$$\psi^0 = \Sigma_R^0 + \Sigma_R^{0c}, \tag{A.13}$$

$$\psi^- = \Sigma_R^- + \Sigma_R^{+c}. \tag{A.14}$$

Finally, we can write the Eq. (A.12) in terms of ψ^0 and ψ^- as

$$\begin{aligned}
& \frac{i}{2} \text{Tr}[\overline{\Sigma}_R \not{D} \Sigma_R] + \frac{i}{2} \text{Tr}[\overline{\Sigma}_R^c \not{D} \Sigma_R^c], \\
&= \frac{i}{2} \overline{\psi^0} \not{\partial} \psi^0 + i \overline{\psi^-} \not{\partial} \psi^- - g \left(\overline{\psi^-} \gamma^\mu \psi^0 W^- + h.c. \right) + g \overline{\psi^-} \gamma^\mu \psi^- W_\mu^3. \tag{A.15}
\end{aligned}$$

Furthermore, we can also simplify the mass terms in Eq. (A.2) as well using the expressions of Σ_R and Σ_R^c (Eqs. (2.1 and A.5)) and considering M_Σ real, i.e.

$$\begin{aligned}
& -\frac{1}{2} \text{Tr}[\overline{\Sigma}_R^c M_\Sigma \Sigma_R] - \frac{1}{2} \text{Tr}[\overline{\Sigma}_R M_\Sigma \Sigma_R^c] \\
&= -\frac{M_\Sigma}{2} \left(\overline{\Sigma}_R^0 \Sigma_R^{0c} + \overline{\Sigma}_R^- \Sigma_R^{+c} + \overline{\Sigma}_R^+ \Sigma_R^- \right) - \frac{M_\Sigma}{2} \left(\overline{\Sigma}_R^{0c} \Sigma_R^0 + \overline{\Sigma}_R^{+c} \Sigma_R^+ + \overline{\Sigma}_R^- \Sigma_R^- \right), \tag{A.16}
\end{aligned}$$

Now, using the relation $\Sigma_R^\pm = C \overline{\Sigma}_R^\pm T$, one can have the following identities

$$\begin{aligned}
\overline{\Sigma}_R^+ \Sigma_R^{-c} &= \overline{\Sigma}_R^- \Sigma_R^{+c}, \\
\overline{\Sigma}_R^{-c} \Sigma_R^+ &= \overline{\Sigma}_R^{+c} \Sigma_R^-. \tag{A.17}
\end{aligned}$$

Therefore, using Eq. (A.17), we can further simplify the mass terms of triplet Σ as

$$\begin{aligned}
& -\frac{1}{2} \text{Tr}[\overline{\Sigma}_R^c M_\Sigma \Sigma_R] - \frac{1}{2} \text{Tr}[\overline{\Sigma}_R M_\Sigma \Sigma_R^c] \\
&= -\frac{M_\Sigma}{2} \left(\overline{\Sigma}_R^0 \Sigma_R^{0c} + \overline{\Sigma}_R^{0c} \Sigma_R^0 \right) - M_\Sigma \left(\overline{\Sigma}_R^- \Sigma_R^{+c} + \overline{\Sigma}_R^{+c} \Sigma_R^- \right), \\
&= -\frac{M_\Sigma}{2} \overline{\psi^0} \psi^0 - M_\Sigma \overline{\psi^-} \psi^-, \tag{A.18}
\end{aligned}$$

while deriving in the last line we have used the definitions of ψ^0 and ψ^- fields given in Eq. (A.13) and Eq. (A.14). Finally, using Eq. (A.15) and Eq. (A.18), we can write the Lagrangian of the triplet field Σ in terms of newly defined two fields ψ^0 and ψ^- as

$$\mathcal{L}_{\text{triplet}} = \frac{i}{2} \text{Tr}[\overline{\Sigma} \not{D} \Sigma] - \frac{1}{2} \text{Tr}[\overline{\Sigma} M_\Sigma \Sigma], \tag{A.19}$$

$$\begin{aligned}
&= \frac{i}{2} \text{Tr}[\overline{\Sigma}_R \not{D} \Sigma_R] + \frac{i}{2} \text{Tr}[\overline{\Sigma}_R^c \not{D} \Sigma_R^c] - \left(\frac{1}{2} \text{Tr}[\overline{\Sigma}_R^c M_\Sigma \Sigma_R] + h.c. \right), \\
&= \frac{i}{2} \overline{\psi^0} \not{\partial} \psi^0 + i \overline{\psi^-} \not{\partial} \psi^- - \frac{M_\Sigma}{2} \overline{\psi^0} \psi^0 - M_\Sigma \overline{\psi^-} \psi^- \\
&\quad - g \left(\overline{\psi^-} \gamma^\mu \psi^0 W^- + h.c. \right) + g \overline{\psi^-} \gamma^\mu \psi^- W_\mu^3. \tag{A.20}
\end{aligned}$$

References

- [1] F. Zwicky, *Die Rotverschiebung von extragalaktischen Nebeln*, *Helv. Phys. Acta* **6** (1933) 110.
- [2] V. C. Rubin and W. K. Ford, Jr., *Rotation of the Andromeda Nebula from a Spectroscopic Survey of Emission Regions*, *Astrophys. J.* **159** (1970) 379.
- [3] D. Clowe, M. Bradac, A. H. Gonzalez, M. Markevitch, S. W. Randall, C. Jones et al., *A direct empirical proof of the existence of dark matter*, *Astrophys. J.* **648** (2006) L109 [[astro-ph/0608407](#)].
- [4] PLANCK collaboration, P. A. R. Ade et al., *Planck 2015 results. XIII. Cosmological parameters*, *Astron. Astrophys.* **594** (2016) A13 [[1502.01589](#)].
- [5] M. Taoso, G. Bertone and A. Masiero, *Dark Matter Candidates: A Ten-Point Test*, *JCAP* **0803** (2008) 022 [[0711.4996](#)].
- [6] LUX collaboration, D. S. Akerib et al., *Results from a search for dark matter in the complete LUX exposure*, *Phys. Rev. Lett.* **118** (2017) 021303 [[1608.07648](#)].
- [7] PANDAX-II collaboration, A. Tan et al., *Dark Matter Results from First 98.7 Days of Data from the PandaX-II Experiment*, *Phys. Rev. Lett.* **117** (2016) 121303 [[1607.07400](#)].
- [8] XENON collaboration, E. Aprile et al., *First Dark Matter Search Results from the XENON1T Experiment*, *Phys. Rev. Lett.* **119** (2017) 181301 [[1705.06655](#)].
- [9] PANDAX-II collaboration, X. Cui et al., *Dark Matter Results From 54-Ton-Day Exposure of PandaX-II Experiment*, *Phys. Rev. Lett.* **119** (2017) 181302 [[1708.06917](#)].
- [10] E. Aprile et al., *Dark Matter Search Results from a One Tonne \times Year Exposure of XENON1T*, [1805.12562](#).
- [11] J. McDonald, *Thermally generated gauge singlet scalars as selfinteracting dark matter*, *Phys. Rev. Lett.* **88** (2002) 091304 [[hep-ph/0106249](#)].
- [12] L. J. Hall, K. Jedamzik, J. March-Russell and S. M. West, *Freeze-In Production of FIMP Dark Matter*, *JHEP* **03** (2010) 080 [[0911.1120](#)].
- [13] J. König, A. Merle and M. Totzauer, *keV Sterile Neutrino Dark Matter from Singlet Scalar Decays: The Most General Case*, *JCAP* **1611** (2016) 038 [[1609.01289](#)].
- [14] A. Biswas and A. Gupta, *Freeze-in Production of Sterile Neutrino Dark Matter in $U(1)_{B-L}$ Model*, *JCAP* **1609** (2016) 044 [[1607.01469](#)].
- [15] A. Biswas and A. Gupta, *Calculation of Momentum Distribution Function of a Non-thermal Fermionic Dark Matter*, *JCAP* **1703** (2017) 033 [[1612.02793](#)].
- [16] N. Bernal, M. Heikinheimo, T. Tenkanen, K. Tuominen and V. Vaskonen, *The Dawn of FIMP Dark Matter: A Review of Models and Constraints*, *Int. J. Mod. Phys.* **A32** (2017) 1730023 [[1706.07442](#)].
- [17] M. Fairbairn and J. Zupan, *Dark matter with a late decaying dark partner*, *JCAP* **0907** (2009) 001 [[0810.4147](#)].
- [18] C. Cheung, G. Elor, L. J. Hall and P. Kumar, *Origins of Hidden Sector Dark Matter I: Cosmology*, *JHEP* **03** (2011) 042 [[1010.0022](#)].
- [19] A. D. Medina, *Higgsino-like Dark Matter From Sneutrino Late Decays*, *Phys. Lett.* **B770** (2017) 161 [[1409.2560](#)].
- [20] T. Gherghetta, B. von Harling, A. D. Medina, M. A. Schmidt and T. Trott, *SUSY implications from WIMP annihilation into scalars at the Galactic Center*, *Phys. Rev.* **D91** (2015) 105004 [[1502.07173](#)].

- [21] D. Borah and A. Gupta, *New viable region of an inert Higgs doublet dark matter model with scotogenic extension*, *Phys. Rev.* **D96** (2017) 115012 [[1706.05034](#)].
- [22] E. Ma, *Verifiable radiative seesaw mechanism of neutrino mass and dark matter*, *Phys. Rev.* **D73** (2006) 077301 [[hep-ph/0601225](#)].
- [23] PARTICLE DATA GROUP collaboration, C. Patrignani et al., *Review of Particle Physics*, *Chin. Phys.* **C40** (2016) 100001.
- [24] P. Minkowski, *$\mu \rightarrow e\gamma$ at a Rate of One Out of 10^9 Muon Decays?*, *Phys. Lett.* **B67** (1977) 421.
- [25] R. N. Mohapatra and G. Senjanovic, *Neutrino Mass and Spontaneous Parity Violation*, *Phys. Rev. Lett.* **44** (1980) 912.
- [26] J. Schechter and J. W. F. Valle, *Neutrino Masses in $SU(2) \times U(1)$ Theories*, *Phys. Rev.* **D22** (1980) 2227.
- [27] E. Ma and D. Suematsu, *Fermion Triplet Dark Matter and Radiative Neutrino Mass*, *Mod. Phys. Lett.* **A24** (2009) 583 [[0809.0942](#)].
- [28] J. Hisano, S. Matsumoto, M. M. Nojiri and O. Saito, *Non-perturbative effect on dark matter annihilation and gamma ray signature from galactic center*, *Phys. Rev.* **D71** (2005) 063528 [[hep-ph/0412403](#)].
- [29] J. Hisano, S. Matsumoto, M. Nagai, O. Saito and M. Senami, *Non-perturbative effect on thermal relic abundance of dark matter*, *Phys. Lett.* **B646** (2007) 34 [[hep-ph/0610249](#)].
- [30] C. Garcia-Cely and J. Heeck, *Phenomenology of left-right symmetric dark matter*, [1512.03332](#).
- [31] M. Cirelli, N. Fornengo and A. Strumia, *Minimal dark matter*, *Nucl. Phys.* **B753** (2006) 178 [[hep-ph/0512090](#)].
- [32] S. Choubey, S. Khan, M. Mitra and S. Mondal, *Singlet-Triplet Fermionic Dark Matter and LHC Phenomenology*, *Eur. Phys. J.* **C78** (2018) 302 [[1711.08888](#)].
- [33] P. Chardonnet, P. Salati and P. Fayet, *Heavy triplet neutrinos as a new dark matter option*, *Nucl. Phys.* **B394** (1993) 35.
- [34] R. Foot, H. Lew, X. G. He and G. C. Joshi, *Seesaw Neutrino Masses Induced by a Triplet of Leptons*, *Z. Phys.* **C44** (1989) 441.
- [35] E. Ma, *Pathways to naturally small neutrino masses*, *Phys. Rev. Lett.* **81** (1998) 1171 [[hep-ph/9805219](#)].
- [36] E. Ma and D. P. Roy, *Heavy triplet leptons and new gauge boson*, *Nucl. Phys.* **B644** (2002) 290 [[hep-ph/0206150](#)].
- [37] W. Chao, *Dark matter, LFV and neutrino magnetic moment in the radiative seesaw model with fermion triplet*, *Int. J. Mod. Phys.* **A30** (2015) 1550007 [[1202.6394](#)].
- [38] F. von der Pahlen, G. Palacio, D. Restrepo and O. Zapata, *Radiative Type III Seesaw Model and its collider phenomenology*, *Phys. Rev.* **D94** (2016) 033005 [[1605.01129](#)].
- [39] FERMI-LAT, MAGIC collaboration, M. L. Ahnen et al., *Limits to dark matter annihilation cross-section from a combined analysis of MAGIC and Fermi-LAT observations of dwarf satellite galaxies*, *JCAP* **1602** (2016) 039 [[1601.06590](#)].
- [40] ATLAS collaboration, G. Aad et al., *Observation of a new particle in the search for the Standard Model Higgs boson with the ATLAS detector at the LHC*, *Phys. Lett.* **B716** (2012) 1 [[1207.7214](#)].
- [41] CMS collaboration, S. Chatrchyan et al., *Observation of a new boson at a mass of 125 GeV with the CMS experiment at the LHC*, *Phys. Lett.* **B716** (2012) 30 [[1207.7235](#)].
- [42] K. Griest and D. Seckel, *Three exceptions in the calculation of relic abundances*, *Phys. Rev.* **D43** (1991) 3191.

- [43] J. Edsjo and P. Gondolo, *Neutralino relic density including coannihilations*, *Phys. Rev.* **D56** (1997) 1879 [[hep-ph/9704361](#)].
- [44] G. Belanger, F. Boudjema, A. Pukhov and A. Semenov, *micrOMEGAs 3: A program for calculating dark matter observables*, *Comput. Phys. Commun.* **185** (2014) 960 [[1305.0237](#)].
- [45] L. Lopez Honorez, E. Nezri, J. F. Oliver and M. H. G. Tytgat, *The Inert Doublet Model: An Archetype for Dark Matter*, *JCAP* **0702** (2007) 028 [[hep-ph/0612275](#)].
- [46] L. Lopez Honorez and C. E. Yaguna, *A new viable region of the inert doublet model*, *JCAP* **1101** (2011) 002 [[1011.1411](#)].
- [47] L. Lopez Honorez and C. E. Yaguna, *The inert doublet model of dark matter revisited*, *JHEP* **09** (2010) 046 [[1003.3125](#)].
- [48] A. Arhrib, Y.-L. S. Tsai, Q. Yuan and T.-C. Yuan, *An Updated Analysis of Inert Higgs Doublet Model in light of the Recent Results from LUX, PLANCK, AMS-02 and LHC*, *JCAP* **1406** (2014) 030 [[1310.0358](#)].
- [49] A. Belyaev, G. Cacciapaglia, I. P. Ivanov, F. Rojas and M. Thomas, *Anatomy of the Inert Two Higgs Doublet Model in the light of the LHC and non-LHC Dark Matter Searches*, [1612.00511](#).
- [50] D. Borah, S. Sadhukhan and S. Sahoo, *Lepton Portal Limit of Inert Higgs Doublet Dark Matter with Radiative Neutrino Mass*, [1703.08674](#).
- [51] A. Biswas, D. Majumdar and P. Roy, *Nonthermal two component dark matter model for Fermi-LAT γ -ray excess and 3.55 keV X-ray line*, *JHEP* **04** (2015) 065 [[1501.02666](#)].
- [52] A. Biswas, S. Choubey and S. Khan, *FIMP and Muon ($g - 2$) in a $U(1)_{L_\mu - L_\tau}$ Model*, *JHEP* **02** (2017) 123 [[1612.03067](#)].
- [53] A. Biswas, D. Borah and A. Dasgupta, *A UV Complete Framework of Freeze-in Massive Particle Dark Matter*, [1805.06903](#).
- [54] F. Kahlhoefer, *Review of LHC Dark Matter Searches*, *Int. J. Mod. Phys.* **A32** (2017) 1730006 [[1702.02430](#)].
- [55] B. Penning, *The Pursuit of Dark Matter at Colliders - An Overview*, *J. Phys.* **G45** (2018) 063001 [[1712.01391](#)].
- [56] ATLAS collaboration, M. Aaboud et al., *Search for long-lived charginos based on a disappearing-track signature in pp collisions at $\sqrt{s} = 13$ TeV with the ATLAS detector*, [1712.02118](#).
- [57] B. Fuks, M. Klasen, D. R. Lamprea and M. Rothering, *Gaugino production in proton-proton collisions at a center-of-mass energy of 8 TeV*, *JHEP* **10** (2012) 081 [[1207.2159](#)].
- [58] B. Fuks, M. Klasen, D. R. Lamprea and M. Rothering, *Precision predictions for electroweak superpartner production at hadron colliders with RESUMMINO*, *Eur. Phys. J. C* **73** (2013) 2480 [[1304.0790](#)].
- [59] Y. Cai and A. P. Spray, *Fermionic Semi-Annihilating Dark Matter*, *JHEP* **01** (2016) 087 [[1509.08481](#)].
- [60] D. Borah, B. Karmakar and D. Nanda, *Common Origin of Dirac Neutrino Mass and Freeze-in Massive Particle Dark Matter*, [1805.11115](#).
- [61] G. Bhattacharyya, M. Dutra, Y. Mambrini and M. Pierre, *Freezing-in dark matter through a heavy invisible Z'* , [1806.00016](#).